

Bimodal Evans–Polanyi Relationships in Hydrogen Atom Transfer from C(*sp*³)–H Bonds to the Cumyloxyl Radical. A Combined Time-Resolved Kinetic and Computational Study.

Michela Salamone,^a Marco Galeotti,^a Eduardo Romero-Montalvo,^b Jeffrey Van Santen,^b
Benjamin D. Groff,^c James M. Mayer,^{*,c} Gino A. DiLabio,^{*,b} and Massimo Bietti^{*,a}

^a *Dipartimento di Scienze e Tecnologie Chimiche, Università "Tor Vergata", Via della Ricerca Scientifica, 1 I-00133 Rome, Italy.*

^b *Department of Chemistry, The University of British Columbia, 3247 University Way, Kelowna, British Columbia, Canada, V1V 1V7*

^c *Department of Chemistry, Yale University, 225 Prospect St.
New Haven, CT, USA 06520-8107*

E-mail: james.mayer@yale.edu; Gino.DiLabio@ubc.ca; bietti@uniroma2.it

Abstract. The applicability of the Evans-Polanyi (EP) relationship to HAT reactions from C(*sp*³)–H bonds to the cumyloxyl radical (CumO•) has been investigated. A consistent set of rate constants *k*_H, for HAT from the C–H bonds of 56 substrates to CumO•, spanning a range of more than four orders of magnitude, has been measured under identical experimental conditions. A corresponding set of consistent gas-phase C–H BDEs spanning 26 kcal mol^{–1} has been calculated using the (RO)CBS-QB3 method. The log *k*_H' vs C–H BDE plot shows two distinct EP relationships, one for substrates bearing benzylic and allylic C–H bonds (*unsaturated* group) and the other one, with a steeper slope, for saturated hydrocarbons, alcohols, ethers, diols, amines and carbamates (*saturated* group), in line with the bimodal behavior observed previously in theoretical studies of reactions promoted by other HAT reagents. The parallel use of BDFEs instead of BDEs allows the transformation of this correlation into a linear free energy relationship, analyzed within the framework of the Marcus theory. The Δ*G*[‡]_{HAT} vs Δ*G*[°]_{HAT} plot shows again distinct behaviors for the two groups. A good fit to the Marcus equation is observed only for the saturated group, with λ = 58 kcal mol^{–1}, indicating that with the unsaturated group λ must increase with increasing driving force. Taken together these results provide a qualitative connection between Bernasconi's

Principle of Nonperfect Synchronization and Marcus theory and suggest that the observed bimodal behavior is a general feature in the reactions of oxygen-based HAT reagents with C(*sp*³)–H donors.

Introduction

The Evans-Polanyi (EP) relationship (also known as Bell-Evans-Polanyi relationship) correlates reaction rate constants (or other activation parameters) with bond dissociation enthalpies (BDEs).^{1,2} The relationship is often employed as a mechanistic tool in C–H bond oxidations promoted by radical and radical-like species, where the observation of a correlation is taken as evidence for a C–H bond cleavage step that occurs through hydrogen atom transfer (HAT).^{3,4,5,6,7} From the correlation obtained for the reaction of a given HAT reagent with a series of substrates or, alternatively, of a given substrate with a series of HAT reagents,^{3,8} it is possible to predict rate constants for the corresponding reactions of additional substrates,⁹ as well as derive substrate BDEs or the BDE of the new bond formed by the HAT reagent following abstraction.^{10,11}

In 1982, Tedder discussed the factors governing reactivity and selectivity in atom transfer reactions.¹² He highlighted the relative importance of the strengths of both the bond being broken and the bond being formed, and of polar and steric effects in these processes. Tedder pointed out that in atom transfer reactions by a given radical, the EP relationship will hold when the reaction is accompanied by a small change in polarity on going from the reactants to the associated transition state.¹³ More recently, one of us found that the empirical extra-thermodynamic relationship defined by EP holds quite well for HAT reactions over a wide range of driving force, when comparing similar radicals and similar substrates, for example for HAT from C–H bonds to oxygen centered radicals.^{3a} This work also highlighted the limitations imposed by the difficulty in compiling a consistent set of C–H bond strengths. The same limitation, together with the importance of extending the correlation over a sufficiently broad range of C–H bond strengths, was also evidenced in a recent work by Jackson and coworkers in the case of HAT reactions promoted by high-valent metal oxo species.¹⁴

Tanko and coworkers examined the kinetics for HAT from the C(*sp*³)–H bonds of a series of 22 amine, hydrocarbon, alcohol and ether substrates to the *tert*-butoxyl radical ((CH₃)₃CO•, *t*BuO•).¹⁵ No simple relationship was observed between the log of the HAT rate constant *k*_H normalized by the number of equivalent abstractable hydrogen atoms *n* (i.e. log *k*_H' where *k*_H' = *k*_H/*n*) and the pertinent C–H BDE taken from the literature or, when not available, calculated by density-

functional theory (DFT). Tanko observed very similar k_H' values for the reaction of $t\text{BuO}^\bullet$ with triallylamine and triethylamine, and with toluene and cyclohexane, despite the fact that both substrate couples have $\text{C}(sp^3)\text{--H}$ bonds that differ in strength by 8-10 kcal mol⁻¹. An apparent curvature in the log k_H' vs C–H BDE plot was observed. For substrates with C–H BDEs greater than 92 kcal mol⁻¹, log k_H' decreased with increasing bond strength, whereas for substrates with C–H BDEs smaller than 92 kcal mol⁻¹, log k_H' appeared to be independent of the C–H BDE and to level off at a value of about 6.6. The analysis of the Arrhenius parameters for the different HAT reactions led to the proposal that, at room temperature, most HAT reactions from C–H bonds to $t\text{BuO}^\bullet$ are entropy controlled.

In recent work by Houk and coworkers, a bimodal EP relationship was found through DFT modeling for the $\text{C}(sp^3)\text{--H}$ bond oxidation of a series of 18 substrates promoted by dimethyldioxirane (DMDO).¹⁶ The authors proposed that these reactions proceed through a rate determining HAT step followed by fast OH rebound. By plotting ΔH^\ddagger vs C–H BDE, correlations with different slopes ($\partial\Delta H^\ddagger/\partial H^\circ$) were observed for the oxidation of aliphatic C–H bonds (*saturated* group) and for those of benzylic, allylic, and α - to C=O or C \equiv N C–H bonds (*unsaturated* group). Within the *saturated* group of C–H oxidations by DMDO, $\partial\Delta H^\ddagger/\partial H^\circ = 0.91$, indicating that the energies of the transition states and of the intermediate carbon centered radicals are influenced to almost the same extent by substrate structure. In the *unsaturated* group, however, the transition state energies reflect little of the resonance stabilization of the allylic or benzylic radical products of HAT ($\partial\Delta H^\ddagger/\partial H^\circ = 0.35$). The differences were rationalized on the basis of Bernasconi's Principle of Nonperfect Synchronization (PNS),^{17,18} that the *unsaturated* reactions are characterized by an "imbalanced transition state". Support for this picture was obtained by calculating, within the *unsaturated* group, the bond length of the $\text{C}(sp^2)\text{--C}(sp^3)$ bond connecting the $\text{C}(sp^3)\text{--H}$ bond to be cleaved to the π system both in the transition state and the intermediate radical, which was taken as a measure of developing resonance stabilization. For all members of the group a significantly shorter bond length was observed in the radical as compared to the transition state, in line with increased resonance stabilization along the reaction coordinate. In this study, in contrast with Tedder's indication,¹² no significant deviation from the correlation was observed for substrates characterized by the presence of C–H α - to polar groups.

Interestingly, a reexamination of Tanko's data (Supporting Information (SI), Figures S1 and S2),¹⁵ shows that the $\log k_H'$ vs C–H BDE plot can be roughly divided into separate *saturated* and *unsaturated* groups, analogous to the groupings proposed by Houk.¹⁶ Specifically, substrates where HAT occurs from aliphatic and α - to heteroatom C–H bonds appear to fall along one correlation line, while those for which HAT occurs from benzylic and allylic C–H bonds fall along a different line with a significantly different slope (Figure S2).

The PNS was also invoked by Korzekwa and coworkers to account for the results obtained in a computational study of HAT from the C(*sp*³)–H bonds in a series of 20 substrates to *p*-nitrosophenoxyl radical, taken as a model for the first step in cytochrome P450 mediated hydroxylation reactions.¹⁹ A modest correlation was observed when plotting activation enthalpies ΔH^\ddagger vs reaction enthalpies ΔH_R , where conjugated systems (the *unsaturated* group) were observed to lie above the correlation line, suggesting that with these substrates resonance stabilization of the product radical provides only limited stabilization to the corresponding transition state. The calculated intrinsic barriers associated to the conjugated substrates were observed to be higher than those associated to the unconjugated counterparts, in line with Bernasconi's PNS stating that a product stabilizing factor that develops late along the reaction coordinate always increases the intrinsic barrier.¹⁷ An excellent correlation was obtained by correcting the disproportionate product stabilization by means of a resonance parameter.¹⁹ A valence bond approach that predicts such bimodal behavior based on the delocalization penalty was also described.^{20,21}

In keeping with the common mechanistic rationalization in terms of the PNS that was provided by the Houk¹⁶ and Korzekwa¹⁹ studies, it is important to point out that this principle and its implication of imbalanced or asynchronous transition states is currently being applied to proton coupled electron transfer (PCET) processes involving C–H,^{22,23,24} O–H and N–H bonds.²⁵ Such processes are increasingly being discussed using a Marcus-theory-type approach, which is based on free energies rather than the enthalpies more traditional for organic HAT reactions. The PNS was primarily discussed in terms of free energies as well.

A critical examination of the studies referenced above,³⁻⁷ shows that the reported correlations are based on a relatively small number of hydrogen atom donor substrates, typically between four and nine. The substrates subjected to study typically contained benzylic or allylic C–H bonds, with limited or no inclusion of substrates bearing unactivated aliphatic C–H bonds (cyclohexane and, to a lesser extent, 2,3-dimethylbutane and cyclooctane). These features prevent a thorough analysis

of the experimental data and a possible assessment of the generality of the bimodal behavior observed for HAT from the C(sp^3)–H bonds of the *saturated* and *unsaturated* substrate groups discussed above.^{15,16,19}

In view of the important role played by HAT reactions from C(sp^3)–H bonds both in chemical and biological processes,^{26,27,28} we sought to develop a deeper understanding of the scope and applicability of the EP relationship to this class of reactions. In keeping with our ongoing interest in HAT reactions involving oxygen centered radicals,²⁹ we compiled from our previous work and carried out additional detailed time-resolved kinetic studies in acetonitrile solution of the reactions of the cumyloxyl radical (PhC(CH₃)₂O•, CumO•) with an extended series of hydrogen atom donor substrates (structures **1-56** displayed below in Table 1 and Table 2). The substrates were selected to cover the broadest possible variety of C(sp^3)–H bonds (unactivated aliphatic, benzylic and allylic, α - to heteroatom (O, N), formylic and α - to an electron withdrawing functional group) and associated bond strengths. CumO• is a well-established HAT reagent and an ideal radical probe for the direct measurement of HAT rate constants by nanosecond laser flash photolysis (LFP) over a broad reactivity range.³⁰

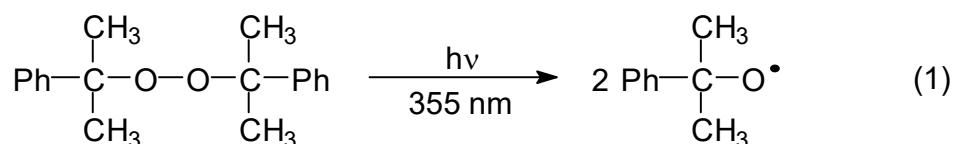
In the present work, C–H BDE values were initially taken from Luo's most recent compilation of chemical bond energies.³¹ However, because of the lack of C–H BDEs for some of the substrates used in this study, the large discrepancy between the available values for some substrates, and the large difference between the available values for some structurally related substrates, we decided instead to calculate the gas-phase C–H BDEs for all substrates. We used the (RO)CBS-QB3 method and, where feasible, also used W1BD for benchmarking purposes. Below we compare these results to the data taken from Luo's compilation. Because one of us has advocated the use of bond dissociation *free energies* (BDFEs) instead of BDEs,^{3b} we have also calculated the gas-phase C–H BDFEs for all substrates (see Supporting Information).

Our approach provides a consistent set of experimental k_H values for HAT from the most activated C–H bonds of substrates **1-56** to CumO•, measured under identical conditions, and a corresponding set of consistent C–H BDEs and BDFEs. These data allow a detailed exploration of the applicability of the EP relationship to HAT reactions from the C–H bonds of an extensive set of hydrogen atom donor substrates, with k_H values spanning a range of more than four orders of magnitude and C–H BDEs spanning a range of 26 kcal mol^{–1}. Moreover, the parallel use of BDFEs

instead of BDEs allows the transformation of this correlation into a linear free energy relationship that can be conveniently analyzed within the framework of the Marcus theory. We also briefly connect this work to prior analyses using valence bond state-correlation diagrams (VBSCDs).

Results

I. Time-resolved kinetic studies. CumO• was generated by 355 nm laser flash photolysis (LFP) of nitrogen or argon-saturated acetonitrile or 2,2,4-trimethylpentane (isooctane) solutions ($T = 25$ °C) containing 1.0 M dicumyl peroxide (eq 1).





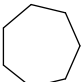
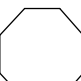
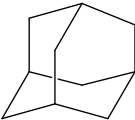

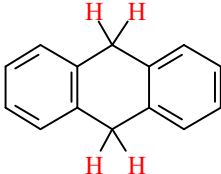
In aprotic solvents, CumO• is characterized by a broad absorption band in the visible region of the spectrum centered at 485 nm.³⁰ Under these conditions, CumO• decays mainly by C–CH₃ β-scission. The reactions of CumO• with the different hydrogen atom donor substrates were studied using the LFP technique. Care was taken to select substrates containing equivalent aliphatic C–H bonds or, in those containing non-equivalent aliphatic C–H bonds, substrates from which HAT to CumO• predominantly or almost exclusively occurs from a single C–H site or type of site. Previous studies clearly show that *tert*-alkoxyl radicals display very low reactivity toward the C–H bonds of unactivated methyl groups ($k_{\text{H}} < 1 \times 10^4 \text{ M}^{-1} \text{ s}^{-1}$),^{32,33} and are essentially unreactive toward alkenyl and aryl C(*sp*²)–H bonds.^{33,34} HAT from primary and secondary amines and alcohols is known to occur predominantly at C–H bonds α to the heteroatom rather than from the N–H and O–H bonds, respectively.^{35,36}

The kinetic measurements were carried out by LFP in acetonitrile by following the decay of the CumO• visible absorption band as a function of substrate concentration. Because of the poor solubility of adamantane (**9**) in acetonitrile, the reaction of CumO• with this substrate was studied in isooctane. The observed rate constants (k_{obs}) gave excellent linear relationships when plotted against substrate concentration (typical r^2 values > 0.99), with intercepts close to that for CumO• β-scission. The second-order rate constants for HAT (k_{H}) were obtained from the slopes of these

plots (see the SI). The k_H values thus obtained for the reaction of CumO• with alkanes and cycloalkanes (substrates **1-9**), and with benzylic and allylic hydrocarbons (substrates **10-16**) are collected in Table 1. Table 2 contains the k_H values measured for reaction of CumO• with alcohols, ethers, diols (substrates **17-28**) and amines (substrates **29-47**), and with *N*-tert-butoxycarbonylpyrrolidine (*N*-Boc-pyrrolidine, **48**), *N*-Boc-L-proline (**49**), benzaldehyde (**50**), hexamethylphosphoric acid triamide (HMPA, **51**), dichloromethane (**52**), chloroform (**53**), dimethylsulfoxide (DMSO, **54**), acetone (**55**) and acetonitrile (**56**). In both tables, the C–H bonds undergoing HAT to CumO• are highlighted in red. All of the sp^3 C–H bonds in substrates **5-8**, **10**, **13-16**, **23**, **24**, **28**, **37-39**, **45**, **47**, **51-56** are equivalent. HAT from tetrahydrofuran (**27**) to CumO• predominantly occurs from four equivalent α -C–H bonds. HAT from cyclohexyl amine (**40**), from cyclic and bicyclic amines (**41-44**, **46**) and from *N*-Boc-pyrrolidine (**48**) to CumO• occurs almost exclusively from the C–H bonds that are α - to the nitrogen atom.^{35,37,38} HAT from *N*-Boc-L-proline (**49**) has been shown to occur selectively from the δ -C–H bonds.³⁸ HAT from benzaldehyde (**50**) occurs selectively from the formyl C–H bond.³⁹ Also included in Table 1 and Table 2 are the k_H' values, obtained by dividing the measured k_H value by the number of equivalent abstractable hydrogen atoms, n ($k_H' = k_H/n$).

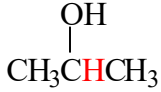
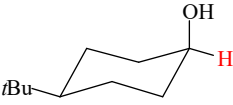
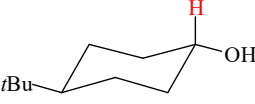
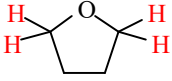
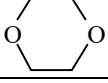
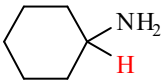
For adamantane (**9**), the partial rate constants for HAT from the secondary and tertiary C–H bonds were derived from the product distribution observed after reaction of CumO• with this substrate in oxygen-saturated isooctane solution (for details see the SI). Under these experimental conditions, the reaction of adamantane led to the formation of products derived from secondary C–H bond oxidation (2-adamantanone) and tertiary C–H bond oxidation (1-adamantanol and 1,3-adamantanediol) in a 0.31 ratio. This result is in excellent agreement with the product ratio determined previously for HAT from adamantane to *t*BuO• (0.28),⁴⁰ and is in line with the almost identical HAT reactivity displayed by these two *tert*-alkoxyl radicals.³⁵ By taking into account the measured k_H value for HAT from adamantane to CumO•, $k_H = 6.90 \times 10^6 \text{ M}^{-1} \text{ s}^{-1}$, and the number of secondary and tertiary C–H bonds, the partial rate constants for HAT from the secondary and tertiary C–H bonds of adamantane can be obtained as $k_H'(\text{sec}) = 1.37 \times 10^5 \text{ M}^{-1} \text{ s}^{-1}$ and $k_H'(\text{tert}) = 1.30 \times 10^6 \text{ M}^{-1} \text{ s}^{-1}$.

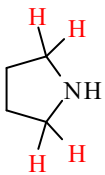
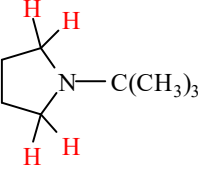
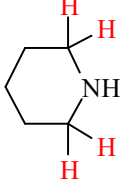
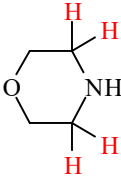
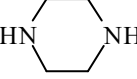
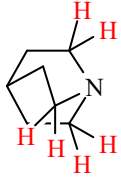

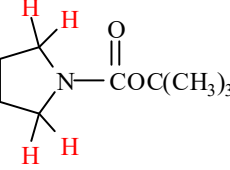
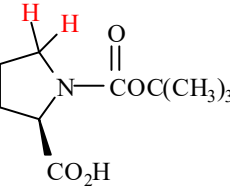
Table 1. Second-Order Rate Constants (k_H) for Reaction of the Cumyloxyl Radical (CumO•) with Hydrocarbon Substrates.

	Substrate	$k_H / \text{M}^{-1} \text{s}^{-1} \text{ }^a$	$k_H' / \text{M}^{-1} \text{s}^{-1} \text{ }^b$	ref.
Aliphatic				
1	<chem>CH3(CH2)3CH3</chem>	$3.1 \pm 0.3 \times 10^5$	5.2×10^4	41
2	<chem>(H3C)3CCCH2CH3</chem>	$9.5 \pm 0.3 \times 10^4$	4.8×10^4	this work
3	<chem>(H3C)2CHCH(CH3)2</chem>	$5.6 \pm 0.2 \times 10^5$	2.8×10^5	this work
4	<chem>(H3C)3CCH(CH3)2</chem>	$2.2 \pm 0.2 \times 10^5$	2.2×10^5	this work
5		$9.54 \pm 0.08 \times 10^5$	9.54×10^4	42
6		$1.1 \pm 0.1 \times 10^6$	9.2×10^4	43
7		$2.20 \pm 0.02 \times 10^6$	1.57×10^5	this work
8		$3.2 \pm 0.1 \times 10^6$	2.00×10^5	41
9		$6.90 \pm 0.07 \times 10^6 \text{ }^c$	$(tert) 1.30 \times 10^6 \text{ }^d$ $(sec) 1.37 \times 10^5 \text{ }^d$	this work
benzylic and allylic				
10	<chem>PhCH3</chem>	$1.85 \pm 0.08 \times 10^5$	6.3×10^4	this work
11	<chem>PhCH2CH3</chem>	$7.9 \pm 0.1 \times 10^5$	4.0×10^5	this work
12	<chem>PhCH(CH3)2</chem>	$5.6 \pm 0.3 \times 10^5$	5.6×10^5	this work
13	<chem>PhCH2Ph</chem>	$8.71 \pm 0.03 \times 10^5$	4.36×10^5	this work
14	<chem>Ph3CH</chem>	$3.04 \pm 0.08 \times 10^5$	3.04×10^5	this work
15		$6.56 \pm 0.03 \times 10^7$	1.64×10^7	44
16		$5.04 \pm 0.01 \times 10^7$	1.26×10^7	this work

^aMeasured in Ar or N₂-saturated MeCN solution at $T = 25 \text{ }^\circ\text{C}$ by 355 nm LFP, [dicumyl peroxide] = 1.0 M. k_H values were determined from the slope of the k_{obs} vs [substrate] plots, where in turn k_{obs} values were measured following the decay of the CumO• visible absorption band at 490 nm. Average of at least two determinations. ^b $k_H' = k_H/n$, where n represents the number of equivalent abstractable hydrogen atoms. ^cMeasured in isooctane solution. ^dDerived from the measured k_H value, taking into account the product distribution observed after reaction of CumO• with adamantane in oxygen-saturated isooctane solution (see text).

Table 2. Second-Order Rate Constants (k_H) for Reaction of the Cumyloxyl Radical (CumO•) with Different Substrates.

	Substrate	$k_H / \text{M}^{-1} \text{s}^{-1} \text{ }^a$	$k_H' / \text{M}^{-1} \text{s}^{-1} \text{ }^b$	ref.
alcohols, ethers and diols				
17	$\text{CH}_3\text{CH}_2\text{OH}$	$1.15 \pm 0.01 \times 10^6$	5.08×10^5	45
18	$\text{CH}_3\text{CH}_2\text{CH}_2\text{OH}$	$1.04 \pm 0.04 \times 10^6$	5.02×10^5	45
19		$2.02 \pm 0.05 \times 10^6$	2.02×10^6	45
20	$\text{HOCH}_2\text{CH}_2\text{OH}$	$8.4 \pm 0.1 \times 10^5$	$4.2 \times 10^5 \text{ }^c$	45
21	$\text{HOCH}_2\text{CH}_2\text{CH}_2\text{OH}$	$1.95 \pm 0.05 \times 10^6$	$9.8 \times 10^5 \text{ }^c$	45
22	$(\text{CH}_3\text{CH}_2)_2\text{O}$	$2.57 \pm 0.03 \times 10^6$	6.5×10^5	this work
23	PhCH_2OH	$2.97 \pm 0.02 \times 10^6$	1.49×10^6	this work
24	$\text{PhCH}_2\text{OCH}_2\text{Ph}$	$5.62 \pm 0.02 \times 10^6$	1.41×10^6	41
25		$5.06 \pm 0.03 \times 10^6$	5.06×10^6	45
26		$2.37 \pm 0.02 \times 10^6$	2.37×10^6	45
27		$5.8 \pm 0.1 \times 10^6$	1.45×10^6	43
28		$8.2 \pm 0.2 \times 10^5$	1.03×10^5	this work
amines				
29	$\text{CH}_3\text{CH}_2\text{CH}_2\text{NH}_2$	$1.10 \pm 0.02 \times 10^7$	5.05×10^6	this work
30	$\text{CH}_3(\text{CH}_2)_3\text{CH}_2\text{NH}_2$	$1.55 \pm 0.02 \times 10^7$	7.75×10^6	41
31	$\text{CH}_3(\text{CH}_2)_4\text{CH}_2\text{NH}_2$	$1.68 \pm 0.02 \times 10^7$	8.4×10^6	this work
32	$\text{CH}_3(\text{CH}_2)_6\text{CH}_2\text{NH}_2$	$1.69 \pm 0.02 \times 10^7$	8.45×10^6	this work
33	$(\text{CH}_3\text{CH}_2\text{CH}_2)_2\text{NH}$	$1.01 \pm 0.03 \times 10^8$	2.53×10^7	35
34	$(\text{CH}_3\text{CH}_2\text{CH}_2)_3\text{N}$	$2.3 \pm 0.1 \times 10^8$	3.83×10^7	46
35	$(\text{CH}_3)_2\text{CHCH}_2\text{NH}_2$	$9.6 \pm 0.1 \times 10^6$	4.8×10^6	35
36	$(\text{CH}_3\text{CH}_2)_3\text{N}$	$2.19 \pm 0.05 \times 10^8$	3.65×10^7	44
37	PhCH_2NH_2	$1.8 \pm 0.1 \times 10^7$	9.0×10^6	35
38	$(\text{PhCH}_2)_2\text{NH}$	$3.75 \pm 0.05 \times 10^7$	9.38×10^6	35
39	$(\text{CH}_2=\text{CHCH}_2)_3\text{N}$	$6.15 \pm 0.06 \times 10^7$	1.03×10^7	46
40		$2.1 \pm 0.1 \times 10^7$	2.1×10^7	41

41		$1.24 \pm 0.05 \times 10^8$	3.1×10^7	37
42		$3.0 \pm 0.1 \times 10^8$	7.5×10^7	37
43		$1.07 \pm 0.01 \times 10^8$	2.68×10^7	37
44		$5.0 \pm 0.2 \times 10^7$	1.25×10^7	37
45		$2.26 \pm 0.01 \times 10^8$	2.83×10^7	37
46		$3.5 \pm 0.2 \times 10^6$	5.8×10^5	this work
47		$1.06 \pm 0.04 \times 10^7$	8.8×10^5	this work
other substrates				
48		$1.4 \pm 0.1 \times 10^7$	3.5×10^6	38
49		$2.51 \pm 0.08 \times 10^6$	1.26×10^6	38
50	PhCHO	$1.23 \pm 0.05 \times 10^7$	1.23×10^7	this work

51	O=P[N(CH ₃) ₂] ₃	1.87±0.02 × 10 ⁷ ^c	1.04 × 10 ⁶	47
52	CH ₂ Cl ₂	6.0±0.2 × 10 ⁴	3.0 × 10 ⁴	this work
53	CHCl ₃	7.7±0.4 × 10 ⁴	7.7 × 10 ⁴	this work
54	$\begin{array}{c} \text{O} \\ \\ \text{H}_3\text{CSCCH}_3 \end{array}$	1.8±0.1 × 10 ⁴	3 × 10 ³	47
55	$\begin{array}{c} \text{O} \\ \\ \text{H}_3\text{CCCH}_3 \end{array}$	< 1 × 10 ⁴	< 2 × 10 ³	47
56	CH ₃ CN	< 1 × 10 ⁴ ^d	< 3 × 10 ³	30

^aMeasured in Ar or N₂-saturated MeCN solution at $T = 25$ °C by 355 nm LFP, [dicumyl peroxide] = 1.0 M. k_{H} values were determined from the slope of the k_{obs} vs [substrate] plots, where in turn k_{obs} values were measured following the decay of the CumO• visible absorption band at 490 nm. Average of at least two determinations. ^b $k_{\text{H}}' = k_{\text{H}}/n$, where n represents the number of equivalent abstractable hydrogen atoms. ^cCalculated considering $n = 2$ based on the difference between the C–H BDEs of the two methylene groups in a intramolecular hydrogen bonded structure (see text). ^dMeasured in isooctane solution.

The k_{H} values for HAT to CumO• displayed in Table 1 and Table 2 span a range of more than four orders of magnitude. On the low end of the range are substrates such as acetone (**55**) and acetonitrile (**56**), which contain electron poor C–H bonds that are strongly deactivated toward HAT to the electrophilic CumO•.^{30,48} With these two substrates, we could only determine an upper limit to k_{H} ($< 1 \times 10^4 \text{ M}^{-1} \text{ s}^{-1}$). On the high end of the range ($k_{\text{H}} \sim 1\text{-}3 \times 10^8 \text{ M}^{-1} \text{ s}^{-1}$) are substrates such as tertiary alkylamines, which contain electron rich and strongly activated α -C–H bonds.^{15,35,37,49}

Figure 1 shows the plot of $\log k_{\text{H}}'$ vs C–H BDE for reaction of CumO• with most of the substrates displayed in Table 1 and Table 2. BDE values are those recommended in Luo's compilation.³¹ For substrates where Luo provides more than one value without a recommendation, the BDE was taken as the average of the tabulated values. Luo's compilation does not contain BDE values for the tertiary C–H bond of 2,2,3-trimethylbutane (**4**), the C–H bonds α - to the OH, NH₂ or NH groups of 1,3-propanediol (**21**), *cis*-4-*tert*-butylcyclohexanol (**25**), *trans*-4-*tert*-butylcyclohexanol (**26**), isobutylamine (**35**) dibenzylamine (**38**), *N-tert*-butylpyrrolidine (**42**), *N*-Boc-pyrrolidine (**48**) and *N*-Boc-proline (**49**), and these substrates were omitted from the plot. The C–H BDE values for HMPA (**51**) and DMSO (**54**), 94.4 and 102.1 kcal mol⁻¹, respectively, were taken from our recent work in which we discussed the large discrepancy between Luo's tabulated value for DMSO of 94.0 kcal mol⁻¹ and our computed value.⁴⁷ The BDE for the α -C–H bonds of hexylamine (**31**) and

octylamine (**32**) are assumed to be identical to the tabulated value for pentylamine (**30**).³¹ The BDE for the α -C–H bonds of dipropylamine (**33**) is assumed to be identical to the tabulated value for tripropylamine (**34**).³¹ All the data employed for the $\log k_H'$ vs C–H BDE plot displayed in Figure 1 are collected in Table S1 in the SI. For comparison, the O–H BDE of 2-phenylpropan-2-ol (cumyl alcohol), is given by Luo as 104.7 ± 0.2 kcal mol⁻¹,³¹ essentially at the right axis of the plots.

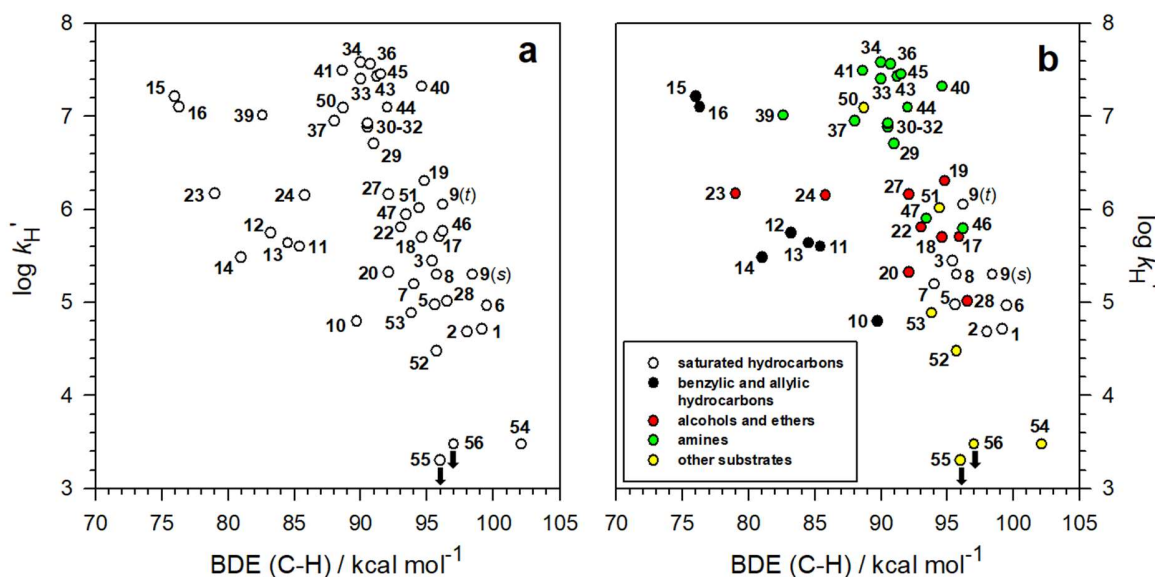



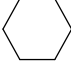

Figure 1. (a) Plot of $\log k_H'$ vs C–H BDE for reaction of the cumyloxyl radical (CumO•) with substrates **1–56**, the structures for which are displayed in Tables 1 and 2. The BDE values are mostly though not entirely from Luo, see text. Substrates **4**, **21**, **25**, **26**, **35**, **38**, **42**, **48**, **49** have been omitted from the plot (see text). The plotted $\log k_H'$ values for **55** and **56** are upper limits. (b) Same plot with kinetic data grouped on the basis of substrate type.

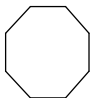
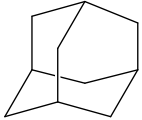
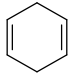
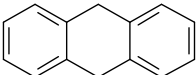
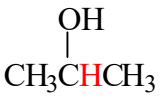
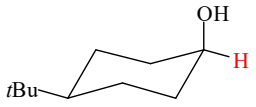
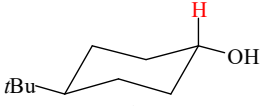
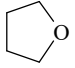
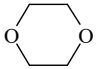
The overall view of Figure 1a suggests that there is not a simple relationship between $\log k_H'$ and C–H BDE. However, grouping the kinetic data based on substrate type, i.e. benzylic/allylic hydrocarbons (black circles), saturated hydrocarbons (white circles), alcohols and ethers (red circles), amines (green circles) and other substrates (yellow circles), reveals two broad relationships (Figure 1b), that are similar to those observed by Tanko and coworkers for HAT reactions involving *t*BuO• with their smaller set of substrates (SI, Figure S2).¹⁵ However, unlike the results of Tanko, the plot displayed in Figure 1b shows no leveling off of $\log k_H'$ at around 6.6. Analysis of the data points displayed in Figure 1b shows that benzyl alcohol (**23**) and dibenzyl ether (**24**) do not follow the same general trend established by the alcohol and ether substrates, nor

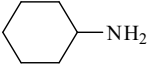
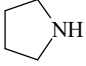
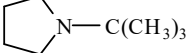
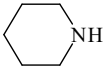
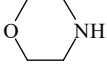



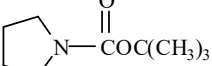
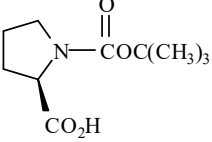
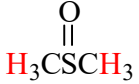
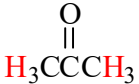
does triallylamine (**39**) fit the general trend associated with the amine substrates. Given their very weak C–H bonds, these substrates would have been expected to react with *much* higher rate constants. HAT from **23**, **24**, and **39** to CumO• occurs selectively from the benzylic and allylic C–H bonds and the corresponding log k_H' values appear to fit fairly well to the benzylic/allylic correlation (black circles).

II. Computations of a Consistent Set of BDEs and BDFEs. One would reasonably expect very similar BDEs for the benzylic C–H bonds of benzyl alcohol (**23**) and dibenzyl ether (**24**), but quite surprisingly the tabulated values differ by 6.8 kcal mol^{−1}, viz. 79.0 and 85.8 kcal mol^{−1},³¹ respectively. From this perspective, the tabulated BDE of 88.0 kcal mol^{−1} for the benzylic C–H bonds of benzylamine (**37**) seems to be too high.³¹ These apparent discrepancies in the BDEs, along with the absence of BDE values for the C–H bonds of some of the substrates listed in Tables 1 and 2, prompted us to use computational methods to generate a consistent set of gas-phase C–H BDEs for substrates **1-56**. We calculated the relevant C–H BDEs using the (RO)CBS-QB3 approach and present these data in Table 3 (column 4). For comparison, Luo’s tabulated values are shown in column 3 of Table 3. According to the benchmarking data we present in the SI, the (RO)CBS-QB3 approach predicts BDEs that are in excellent agreement with the BDEs we computed for 22 out of the 56 substrates using the high-level W1BD approach (mean absolute error, MAE = 0.26 kcal mol^{−1}). Additional analysis of the calculated BDEs is provided in the SI.

Table 3. BDE and BDFE Values for the Pertinent C–H Bonds of Substrates **1-56**.

		C–H BDE (kcal mol ^{−1})		C–H BDFE (kcal mol ^{−1})
	substrate	Luo ^a	this work ^b	this work ^b
1	CH ₃ (CH ₂) ₃ CH ₃	99.15 ^c	99.1	89.5
2	(H ₃ C) ₃ CCCH ₂ CH ₃	98.0	99.3	89.4
3	(H ₃ C) ₂ CHCH(CH ₃) ₂	95.4	96.9	86.7
4	(H ₃ C) ₃ CCCH(CH ₃) ₂	<i>n.a.</i>	97.0	86.7
5		95.6	96.3	88.8
6		99.5	99.3	90.3
7		94.0	95.8	86.7

8		95.7	94.2	85.4
9		96.2 (<i>tert</i>) 98.4 (<i>sec</i>)	100.1 (<i>tert</i>) 100.5 (<i>sec</i>)	91.5 (<i>tert</i>) 91.5 (<i>sec</i>)
10	PhCH ₃	89.7	89.7	83.1
11	PhCH ₂ CH ₃	85.4	87.6	79.1
12	PhCH(CH ₃) ₂	83.2	86.9	77.4
13	PhCH ₂ Ph	84.5	82.8	76.5
14	Ph ₃ CH	81.0	82.2	74.7
15		76.0	75.0	66.9
16		76.3	78.6	68.8
17	CH ₃ CH ₂ OH	95.9	95.2	86.6
18	CH ₃ CH ₂ CH ₂ OH	94.6	95.7	87.1
19		94.8	94.4	85.5
20	HOCH ₂ CH ₂ OH	92.1	95.1 ^d	86.8 ^d
21	HOCH ₂ CH ₂ CH ₂ OH	<i>n.a.</i>	94.0 ^d	85.7 ^d
22	(CH ₃ CH ₂) ₂ O	93.0	95.5	86.2
23	PhCH ₂ OH	79.0	83.2	74.6
24	PhCH ₂ OCH ₂ Ph	85.8	83.7	74.8
25		<i>n.a.</i>	93.7	85.0
26		<i>n.a.</i>	95.6	87.1
27		92.1	93.8	85.8
28		96.5	97.6	88.4
29	CH ₃ CH ₂ CH ₂ NH ₂	91.0	92.3	83.6
30	CH ₃ (CH ₂) ₃ CH ₂ NH ₂	90.5	92.3	83.6
31	CH ₃ (CH ₂) ₄ CH ₂ NH ₂	<i>n.a.</i> ^e	92.3	83.6
32	CH ₃ (CH ₂) ₆ CH ₂ NH ₂	<i>n.a.</i> ^e	92.3	83.6
33	(CH ₃ CH ₂) ₂ NH	<i>n.a.</i> ^e	92.0	83.1
34	(CH ₃ CH ₂) ₃ N	90.0	91.2	82.4

35	$(\text{CH}_3)_2\text{CHCH}_2\text{NH}_2$	<i>n.a.</i>	92.5	83.8
36	$(\text{CH}_3\text{CH}_2)_3\text{N}$	90.7	91.2	82.8
37	PhCH_2NH_2	88.0	79.8	71.7
38	$(\text{PhCH}_2)_2\text{NH}$	<i>n.a.</i>	79.9	71.7
39	$(\text{CH}_2=\text{CHCH}_2)_3\text{N}$	82.6	81.2	72.6
40		94.6	91.1	82.3
41		88.6	90.7	82.4
42		<i>n.a.</i>	89.3	81.4
43		91.2	92.2	83.5
44		92.0	93.3	84.6
45		91.5	93.5	84.4
46		96.2	98.6	90.1
47		93.4	98.9	90.5
48		<i>n.a.</i>	92.5 ^f	84.1 ^f
49		<i>n.a.</i>	93.6 ($\delta\text{-C-H}$) 88.4 ($\alpha\text{-C-H}$)	85.1 ($\delta\text{-C-H}$) 80.5 ($\alpha\text{-C-H}$)
50	PhCHO	88.7	91.4	82.8
51	$\text{O=P}[\text{N}(\text{CH}_3)_2]_3$	<i>n.a.</i>	93.9 ^g	85.1
52	CH_2Cl_2	95.7	96.3	87.4
53	CHCl_3	93.8	93.7	85.1
54		94.0	102.3 ^g	93.6
55		96.0	96.7	88.7
56	CH_3CN	97.0	96.6	88.3

^aTaken from ref. 31, recommended values (where available). ^bCalculated using the (RO)CBS-QB3 approach (see text). ^cAverage of the recommended values for the C–H bonds at C-2 and C-3 (99.2 and 99.1 kcal mol⁻¹, respectively). ^dBDE and BDFE values for the C–H bonds that are α to the HBD OH group in intramolecular hydrogen bonded structures (see text). ^eIn Figure 1, BDEs for **31** and **32** were taken to be the same as the value for **30**,³¹ the BDE for **33** was assumed to be the same as the value for **34**.³¹ ^fBecause the calculations lead to slightly different BDEs and BDFEs

for the C–H bonds of this substrate that are *cis* and *trans* to the carbonyl group (BDE = 92.6 and 92.3 kcal mol⁻¹, BDFE = 84.2 and 83.9 kcal mol⁻¹ respectively), the given values are an average of the BDEs and BDFEs for the two C–H bond couples. [§]In Figure 1, the BDEs for **51** and **54** were from ref. 47; see text.

Compared to Luo's set of compiled data,³¹ the computed BDE for the benzylic C–H bonds of benzylamine (**37**) is significantly lower (79.8 vs 88.0 kcal mol⁻¹). The computed value is also similar to that obtained for the corresponding C–H bonds of dibenzylamine (**38**). The computed BDEs for the benzylic C–H bonds of benzyl alcohol (**23**) and dibenzyl ether (**24**) are now very similar, in line with expectations (83.2 and 83.7 kcal mol⁻¹, respectively). The computations also produce BDEs for the secondary and tertiary C–H bonds of adamantane (**9**) that are very similar, viz. 100.5 and 100.1 kcal mol⁻¹, respectively.

Interestingly, with 1,2-ethanediol (**20**) and 1,3-propanediol (**21**) calculations predict an intramolecular hydrogen bonded structure that in acetonitrile is more stable than the non-hydrogen bonded one by 2.5 and 3.5 kcal mol⁻¹, respectively (SI, Figure S28). The BDEs for the C–H bonds that are α to the hydrogen bond donor (HBD) and hydrogen bond acceptor (HBA) OH groups are 95.1 and 97.4 kcal mol⁻¹ and 94.0 and 96.0 kcal mol⁻¹, for **20** and **21**, respectively. The corresponding BDFEs are 86.8 and 88.4 kcal mol⁻¹, and 85.7 and 87.2 kcal mol⁻¹. Based on these findings, it can be reasonably assumed that with both substrates HAT to CumO• predominantly occurs from the weaker and more electron rich C–H bonds of a single methylene unit, and accordingly, for these two substrates the k_{H}' values displayed in Table 2 have been obtained considering $n = 2$.

Also included in Table 3 are the computed gas-phase C–H BDFEs for substrates **1-56**, calculated using the (RO)CBS-QB3 approach. The BDFEs are on average 8.6 ± 0.7 kcal mol⁻¹ lower than the corresponding BDEs (uncertainty is 1σ). This difference is primarily due to the entropy of H•(g), $T\Delta S^\circ(\text{H}^\bullet)_{(\text{g})} = 8.17$ kcal mol⁻¹.⁵⁰ The agreement between these values indicates that the entropies of R–H and R• are close to the same.⁵¹ Because there is close to a constant shift between BDE and BDFE, the plots in this report look very similar using either parameter, with just a change in the horizontal axis (see below).

For comparison, the computed O–H BDE and BDFE for cumyl alcohol (2-phenylpropan-2-ol) are 106.6 and 98.2 kcal mol⁻¹.

III. Rate Constant – Bond Strength Correlations. In Figure 2, we plot the measured $\log k_H'$ values for HAT from substrates **1-56** to CumO• taken from Table 1 and Table 2 against the calculated C–H BDEs from Table 3.

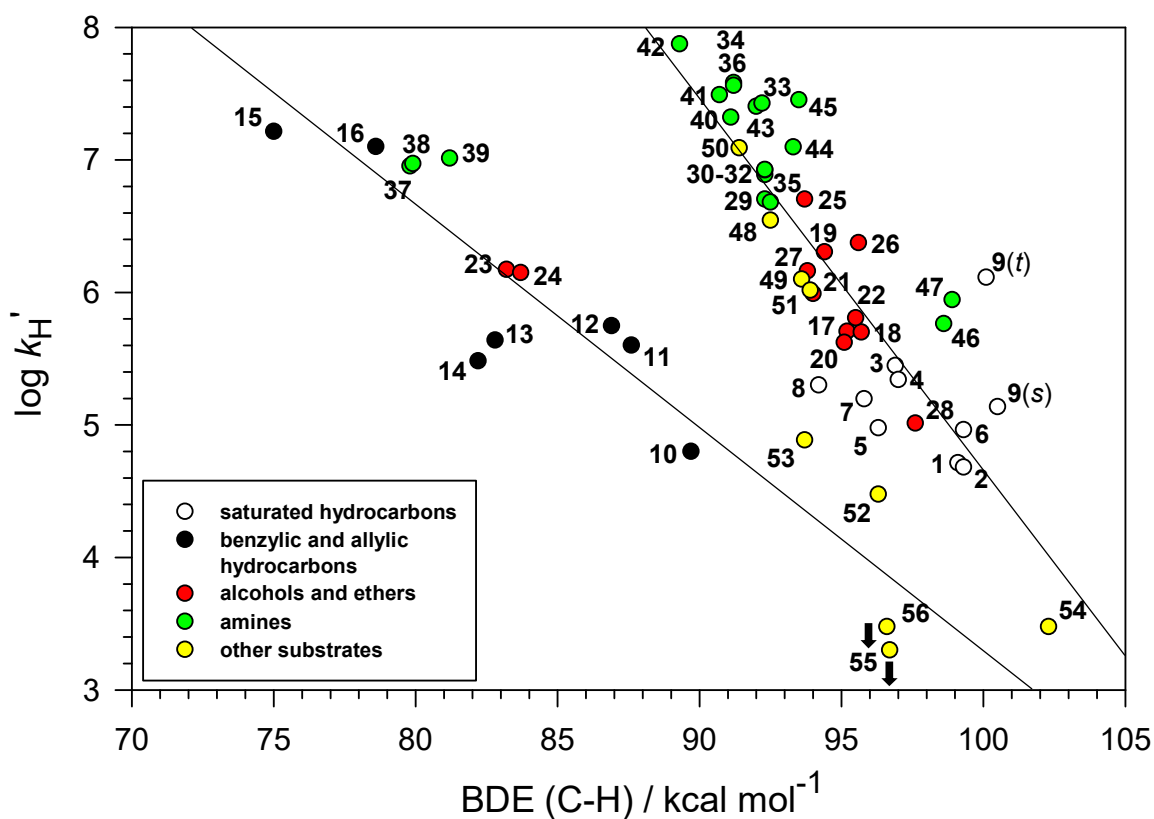


Figure 2. Plot of $\log k_H'$ vs C–H BDEs calculated using the (RO)CBS-QB3 approach, for reaction of the cumyloxyl radical (CumO•) with substrates **1-56**. The $\log k_H'$ values for **55** and **56** are upper limits.

Figure 2 reveals trends in the relationship between $\log k_H'$ and C–H BDE that are not apparent in Figure 1a, clarifying the trends that are roughly present in Figure 1b. Specifically, the data associated with the benzylic and allylic hydrocarbons (black circles), i.e., the *unsaturated* group, show a relatively good correlation, in particular with the inclusion of the data associated with benzyl alcohol (**23**), dibenzyl ether (**24**), benzylamine (**37**), dibenzylamine (**38**) and triallylamine (**39**). Figure 2 also shows that the points for saturated hydrocarbons, alcohols, ethers, diols, amines and carbamates (*saturated* group) tend to cluster around a different line with a slope that is steeper than that associated with the benzylic/allylic set, albeit with a lower correlation coefficient.

Collectively, Figure 2 demonstrates that, depending on the nature of the substrate, there are two distinct EP relationships, and these results provide strong support for the bimodal behavior observed previously in purely theoretical studies of reactions promoted by other HAT reagents.^{16,19}

IV. Correlation of ΔG^\ddagger with ΔG° . Recasting the rate/bond strength relationships in terms of bond dissociation *free energies* (BDFEs) allows plots such as Figure 2 to be viewed as linear free energy relationships and analyzed with a version of Marcus theory. The basic Marcus equation for the reaction barrier depends only on the free energy driving force (ΔG°) and the reorganization energy λ (eq 2). λ is the energy required to reorganize the reactants and their surrounding solvent to the structure of the products without the hydrogen atom transferring. In this model, the barrier at $\Delta G^\circ = 0$ is $\lambda/4$, which is sometimes termed the ‘intrinsic barrier’ ΔG^\ddagger_0 . The Brønsted α is then given by eq 3 (assuming λ does not vary with ΔG° across the series).

$$\Delta G^\ddagger = \frac{(\Delta G^\circ + \lambda)^2}{4\lambda} = \frac{\Delta G^\circ}{2} + \frac{\lambda}{4} + \frac{\Delta G^{\circ 2}}{4\lambda} \quad (2)$$

$$\frac{\partial \Delta G^\ddagger}{\partial \Delta G^\circ} = \frac{1}{2} + \frac{\Delta G^\circ}{2\lambda} \quad (3)$$

The driving force for the HAT reactions, or $\Delta G^\circ_{\text{HAT}}$, is the computed BDFE for the C–H bond minus BDFE(CumO–H) (since free energies of solution are very similar for RH and R•).⁵² The HAT rate constants displayed in Table 1 and Table 2 are converted to $\Delta G^\ddagger_{\text{HAT}}$ with the Eyring equation. The plot of $\Delta G^\ddagger_{\text{HAT}}$ vs $\Delta G^\circ_{\text{HAT}}$ (Figure 3) is a Brønsted plot, equivalent to a plot of $\log k_{\text{H}}'$ vs $\log K_{\text{eq}}$. Again, *saturated* and *unsaturated* classes of substrates fall on two lines that have different slopes. This is not surprising since very similar data is being plotted (with the vertical axis inverted since $\log k_{\text{H}}' \propto -\Delta G^\ddagger_{\text{HAT}}$).

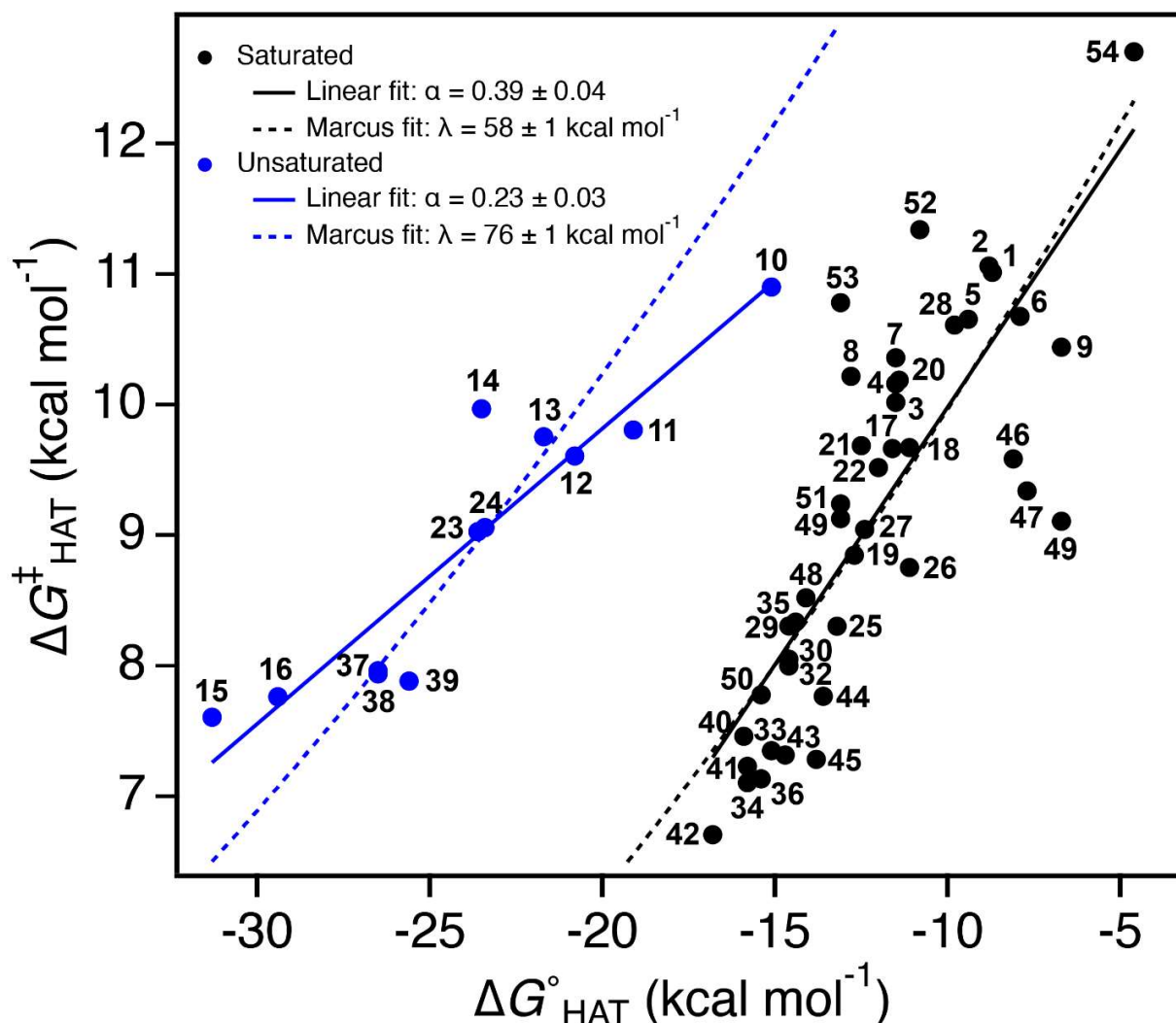


Figure 3. Plot of $\Delta G^\ddagger_{\text{HAT}}$ vs $\Delta G^\circ_{\text{HAT}}$ derived from the data in Tables 1-3 (omitting data for 55 and 56). The black circles are for the *saturated* substrates, and the best linear fit (black solid line) has a Brønsted slope $\alpha = 0.39$ with an intercept $\Delta G^\ddagger_0 = 13.9 \pm 0.6$ kcal mol⁻¹ at $\Delta G^\circ = 0$. The *unsaturated* data are shown in blue, and the fit line has $\alpha = 0.23$ with $\Delta G^\ddagger_0 = 14.3 \pm 0.7$ kcal mol⁻¹ at $\Delta G^\circ = 0$. The best fit to the Marcus equation for the saturated (black dashed curve) and unsaturated (blue dashed curve) substrates, is obtained with $\lambda = 58 \pm 1$ and 76 ± 1 kcal mol⁻¹, respectively.

The slopes of these linear free energy relationships, $\partial \Delta G^\ddagger_{\text{HAT}} / \partial \Delta G^\circ_{\text{HAT}} = \partial \log k_{\text{H}}' / \log K_{\text{eq}} =$ Brønsted α , are unitless and carry some intuition. For the unsaturated compounds (solid blue line), $\alpha = 0.23$, meaning that the barrier is not very sensitive to the driving force: a decrease of 1 kcal mol⁻¹ in $\Delta G^\circ_{\text{HAT}}$ only lowers the barrier by 0.23 kcal mol⁻¹. The saturated line (solid black line) is

steeper, however, with $\alpha = 0.39$. The intercepts of the two lines ΔG^\ddagger_0 at $\Delta G^\circ_{\text{HAT}} = 0$, are 14.3 ± 0.7 and 13.9 ± 0.6 kcal mol⁻¹, for the unsaturated and saturated substrate groups, respectively. The saturated data show a good fit (dashed black curve) to the Marcus equation (eq 2), with $\lambda = 58 \pm 1$ kcal mol⁻¹. In contrast, the best fit for the unsaturated substrates does not match the slope of the data (blue dashed curve, $\lambda = 76 \pm 1$ kcal mol⁻¹).

Discussion

I. k_{H} vs. BDE Correlations. To our knowledge, this is the most extensive experimental dataset that has been assembled to examine rate-bond strength correlations for hydrogen atom transfer. A consistent set of BDEs has been assembled using high-level computations. While there is some scatter and some substrates are outliers, the data clearly sort into two primary categories: *saturated* C–H bonds vs. *unsaturated* (allylic or benzylic) C–H bonds. This separation is clearly seen both in the log k_{H} vs BDE plot and in the data recast as $\Delta G^\ddagger_{\text{HAT}}$ vs $\Delta G^\circ_{\text{HAT}}$ (Figures 2 and 3).

Ia. Outliers from the Correlations. As mentioned above, for acetone (**55**) and acetonitrile (**56**) only an upper limit to k_{H} ($< 1 \times 10^4$ M⁻¹ s⁻¹) could be determined and accordingly these two substrates were excluded from the correlations. The C–H bonds of acetone and acetonitrile (BDE = 96.7 and 96.6 kcal mol⁻¹, respectively) are similar in strength to the tertiary C–H bonds of 2,3-dimethylbutane (**3**) and 2,2,3-trimethylbutane (**4**) (BDE = 96.9 and 97.0 kcal mol⁻¹), but the HAT rate constants for **55** and **56** are at least 70 times lower. The extremely low reactivity of these compounds is typically ascribed to an electronic ‘polar effect’ determined by the electron withdrawing character of the carbonyl and cyano groups.⁴⁸ Such deactivation toward HAT to the electrophilic CumO• prevents the study of substrates bearing C(*sp*³)–H bonds α - to strong electron withdrawing functional groups. Still, it is interesting to note that in Figure 2 the corresponding data points fall significantly closer to the benzylic/allylic correlation line than to the *saturated* one, in agreement with the results obtained in the above mentioned theoretical studies.^{16,19} Thus it is possible that the observed deactivation also has a contribution from the factors that make benzylic and allylic C–H bonds less reactive than saturated compounds with the same BDE (see below).

Significant outliers from the best-fit lines displayed in Figure 2 are observed for both the *saturated* and *unsaturated* groups of substrates. Diphenylmethane (**13**) and triphenylmethane (**14**) are less reactive than expected, perhaps due to steric effects. Removing these two substrates from the fit improves the correlation coefficient from 0.755 to 0.905. The most significant outliers from the

saturated group are adamantane (**9**), 1-azabicyclo[2.2.2]octane (**46**), 1,4-diazabicyclo[2.2.2]octane (**47**), dichloromethane (**52**) and chloroform (**53**). Removing these substrates from the fit improves the correlation coefficient from 0.689 to 0.878.

The measured k_{H}' values for HAT from the α -C–H bonds of 1-azabicyclo[2.2.2]octane (**46**) and 1,4-diazabicyclo[2.2.2]octane (**47**) ($k_{\text{H}}' = 5.8 \times 10^5$ and $8.8 \times 10^5 \text{ M}^{-1} \text{ s}^{-1}$, respectively) are significantly lower than those associated to conformationally non-restricted acyclic and cyclic tertiary amines (for which $k_{\text{H}}' = 3\text{--}4 \times 10^7 \text{ M}^{-1} \text{ s}^{-1}$).^{35,37} This decrease in reactivity was previously explained on the basis of the operation of stereoelectronic effects.^{15,35,49,53} In **46** and **47**, the α -C–H bonds undergoing HAT and the radical formed are held in conformations that prevent optimal overlap with the nitrogen lone pair, minimizing hyperconjugative α -C–H bond weakening and radical stabilization. The computed BDEs (98.6 and 98.8 kcal mol^{−1}, for **46** and **47**, respectively) are about 8 kcal mol^{−1} higher than those obtained for the corresponding bonds of acyclic tertiary amines, suggesting that the operation of stereoelectronic effects is fully reflected therein. Given these much higher C–H BDEs, the k_{H}' values for **46** and **47** are actually higher than expected (positive deviations from the correlation line). The unusually electron rich character of the nitrogen lone pair, which can favor interaction with the electrophilic CumO•, and the rigidity of the bicyclic scaffold of these two substrates (see below) may account for the observed behavior.

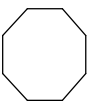
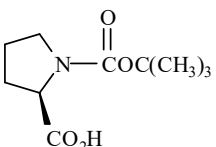
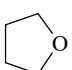
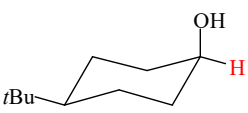
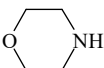
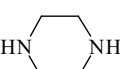
The results for adamantane (**9**) require a dedicated discussion. The secondary C–H BDE for an acyclic alkane substrate and the k_{H}' for HAT from these bonds can be obtained from the average of the values for pentane (**1**) and 2,2-dimethylbutane (**2**) as 99.2 kcal mol^{−1} and $5.0 \times 10^4 \text{ M}^{-1} \text{ s}^{-1}$, respectively (Table 3 and Table 1). Similarly, the tertiary C–H BDE and k_{H}' for HAT from this bond can be obtained from the average of the values for 2,3-dimethylbutane (**3**) and 2,2,3-trimethylbutane (**4**) as 97.0 kcal mol^{−1} and $2.5 \times 10^5 \text{ M}^{-1} \text{ s}^{-1}$, neglecting, to a first approximation, the different accessibility of the secondary C–H bonds of **1** and **2**, and of the tertiary C–H bonds of **3** and **4** determined by steric effects. On the basis of these averaged values, the secondary and tertiary C–H bonds of **9** appear to be 2.7 and 5.2 times more reactive than their acyclic counterparts, despite the fact that their C–H BDEs are higher by 0.9 and 3.5 kcal mol^{−1}, respectively. This is evident in the positive deviation of this substrate (in particular with respect to HAT from the tertiary C–H bonds) from the *saturated* correlation line (Figure 2). This effect can reasonably be explained on the basis of the unhindered nature of the tertiary C–H bonds and the

rigidity of the adamantane scaffold, which should reduce the reorganization energy penalty to form the radical. This deviation likely explains why, to the best of our knowledge, **9** has been never included as a hydrogen atom donor substrate in $\log k_H'$ (or ΔH^\ddagger) vs BDE correlations, even though it is customarily employed as a mechanistic probe in C–H bond oxidation studies.^{54,55}

Removing the aforementioned outliers (namely **13** and **14** for the *unsaturated*, and **9**, **46**, **47**, **52**, and **53** for the *saturated* substrates) from the $\Delta G^\ddagger_{\text{HAT}}$ vs $\Delta G^\circ_{\text{HAT}}$ plot displayed in Figure 3 widens the gap between the Brønsted α values for the two correlations, from 0.23 to 0.22 and 0.39 to 0.51 for the unsaturated and saturated substrates, respectively.

Ib. Polar Effects. The *saturated* substrate group shows a good correlation over a broad range of C(*sp*³)–H bonds, spacing from non-activated to increasingly activated ones such as those α - to electron releasing hydroxyl, alkoxyl and amino groups. With the exception of dichloromethane (**52**) and chloroform (**53**) that display strongly electronically deactivated C–H bonds, the presence of the heteroatom causes only barely visible systematic deviations from the correlation line. For the electron-rich substrates in our dataset, the amines, alcohols and ethers, polar effects seem to enhance the rate constants. The effect is not large enough to confidently see distinct correlation lines for different classes of saturated compounds, especially given the scatter for the different compounds within a class. However, Figure 2 shows that all but two of the amines lie on or above the correlation line, while all of the saturated hydrocarbons lie on or below the correlation line (except for adamantane (**9**), see above). The polar effect is most evident when comparing compounds displaying reactive C–H bonds with similar BDEs, in other words traversing up a vertical line in Figure 2. For essentially every BDE where comparisons can be made, the order of $\log k_H'$ values is hydrocarbons < oxygenates < amines, with very few exceptions. One group of such compounds, with $\text{BDE} = 93.7 \pm 0.5$, is listed in Table 4.

Table 4. Comparison between the normalized rate constants k_H' , for compounds with C–H BDEs of 93.7 ± 0.5 kcal mol⁻¹.

compound		k_H' (M ⁻¹ s ⁻¹)	k_H' (rel)	BDE C–H (kcal mol ⁻¹)
53	CHCl ₃	7.7×10^4	1.0	93.7
8		2.00×10^5	2.6	94.2
21	HOCH ₂ CH ₂ CH ₂ OH	9.8×10^5	12.7	94.0
51	O=P[N(CH ₃) ₂] ₃	1.04×10^6	13.5	93.9
49		1.26×10^6	16.4	93.6
27		1.45×10^6	18.8	93.8
25		5.06×10^6	65.7	93.7
44		1.25×10^7	162	93.3
45		2.83×10^7	368	93.5

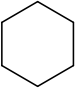
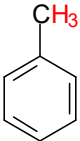
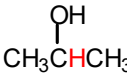
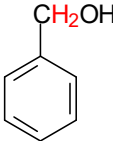
Within this series, chloroform (**53**) displays the lowest k_H' value, in line with the strong C–H bond deactivation determined by the presence of the three electron withdrawing chlorine atoms. The 142-fold difference between cyclooctane (**8**) and piperazine (**45**) is much larger than the factor of ca. 5 expected for the 1 kcal mol⁻¹ difference in BDE between the C–H bonds of these saturated substrates. Thus, the amines react faster than expected even after considering the C–H bond weakening due to hyperconjugation with the nitrogen lone pair. This enhanced reactivity resulting from the neighboring N or O contrasts with the lower reactivity of significantly weaker benzylic and allylic C–H bonds where the product radical can be delocalized over neighboring vinyl or aryl groups. If spin delocalization onto N in the amine substrates were similar to its delocalization in the unsaturated substrates, then the green points in Figure 2 would likely fall between the two correlation lines, not on or above the line for saturated substrates.

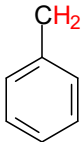
N-Boc-proline (**49**) provides a striking example of the important role played by polar effects in these reactions.³⁸ HAT to CumO• selectively occurs from the δ -C–H bonds next to the N center,⁵⁶ despite the fact that computations indicate that these bonds are stronger than the tertiary α -C–H one by 5.2 kcal mol⁻¹. Polar effects resulting from the presence of the CO₂H group, account for α -C–H bond deactivation, while the carbamate nitrogen atom is still sufficiently electron rich to activate the δ -C–H bonds toward HAT.

The *unsaturated* compounds similarly fall close to a correlation line, which covers a similar range of k_{H}' values at significantly weaker C–H bonds and has a shallower slope. The amines, alcohol and ether that are allylic or benzylic fall on this unsaturated line, rather than with the saturated amines or oxygenates.

The observed behavior is nicely exemplified by comparing reactions from the two groups with similar k_{H}' values but significantly different C–H BDEs (Scheme 1). In all the examples shown, for hydrocarbons, alcohols and amines, the 9-13 kcal mol⁻¹ lower BDEs for the benzylic or allylic C–H bonds remarkably do not lead to higher rate constants than their saturated counterparts. A similar pattern has been observed in HAT reactions promoted by other oxygen-centered abstractors such as the *tert*-butylperoxyl radical (*t*BuOO•) and photoexcited decatungstate),^{28b,57} as well as in the experimental study of HAT to *t*BuO• by Tanko,¹⁵ and the computational one of HAT to DMDO by Houk,¹⁶ supporting the generality of these conclusions.

Scheme 1. Comparison between C–H BDEs of different substrate groups with similar normalized HAT rate constants, k_{H}' .

	<chem>CH3(CH2)3CH3</chem>				
k_{H}' (M ⁻¹ s ⁻¹)	5.2 x 10⁴	9.2 x 10⁴	6.3 x 10⁴	2.0 x 10⁶	1.5 x 10⁶
BDE C–H (kcal mol ⁻¹)	99.1	99.3	89.7	94.4	83.2

	<chem>CH3(CH2)3CH2NH2</chem>		<chem>(CH3CH2)3N</chem>	<chem>(CH2=CHCH2)3N</chem>
k_H^* ($M^{-1} s^{-1}$)	7.8×10^6	9.0×10^6	3.7×10^7	1.0×10^7
BDE C–H ($kcal\ mol^{-1}$)	92.3	79.8	91.2	81.2

II. The Principle of Nonperfect Synchronization as the Origin of the Higher Intrinsic Barriers for Unsaturated Substrates. The sorting of the experimental rate constants for C–H abstraction by CumO• into *saturated* vs. *unsaturated* substrates is a deviation from the simple Evans-Polanyi (EP) correlation discussed above. This sorting is similar to that made in the theoretical study by Houk and coworkers of C(*sp*³)–H bond oxidations promoted by DMDO.¹⁶ A similar pattern was seen in early theoretical calculations on HAT reactions from C(*sp*³)–H bonds to the *p*-nitrosophenoxyl radical, where higher intrinsic barriers were suggested for conjugated substrates as compared to the unconjugated counterparts.¹⁹ In the computational DMDO study, the bimodal EP relationships separated the oxidations of C–H bonds that were aliphatic or α-, β-, γ- and δ- to an oxygen atom (saturated) from those that were benzylic, allylic, or α- to C=O or C≡N (unsaturated). Houk et al. explained this separation on the basis of Bernasconi's Principle of Nonperfect Synchronization (PNS),¹⁷ by suggesting that with the unsaturated substrates, resonance stabilization of the product radical is proportionally greater than that for the corresponding transition state.

An analogous PNS explanation can be put forward in the present study, in order to account for the bimodal EP relationship observed for HAT from the C(*sp*³)–H bonds of substrates **1–56** to CumO• (Figure 2), grouped analogously. The product stabilizing factor that lowers the BDE—resonance stabilization—develops late along the reaction coordinate, mostly after the transition state. Because the transition state is not proportionally as stabilized as would have been expected on the basis of the BDE, the rates for the resonance stabilized compounds are slower than expected. The shallower slope observed for the *unsaturated* substrate group is indicative of reactions characterized by an even more imbalanced transition state, where the relative importance of benzylic or allylic resonance stabilization increases on going from the HAT transition state to the product radical (see below). The results reported here and in the Houk theoretical study, together

with prior work, suggest that the division in terms of *saturated* and *unsaturated* substrates could represent a general feature in the reactions of oxygen-based HAT reagents with C(sp³)-H donors.

III. Slopes of the Correlation Lines. The slopes of the correlation lines displayed in Figure 3 provide insights beyond the sorting of *saturated* vs. *unsaturated* substrates. The *unsaturated* group falls on a distinctly shallower line, with a unitless slope $\alpha = 0.23$ for $\partial\Delta G^\ddagger/\partial\Delta G^\circ$. A shallow slope is also observed in Houk’s computational dataset, with $\alpha = 0.35$ for $\partial\Delta H^\ddagger/\partial\Delta H^\circ$. The slopes for the *saturated* compounds are both larger, but quite different for the two studies: $\alpha_{\text{saturated}} = 0.39$ for CumO• vs. 0.91 for DMDO. These differences in slope could reflect differences in the ranges of driving forces, for instance the large α value for HAT from *saturated* substrates to DMDO reflecting that all of the reactions considered in that group were endothermic. The more exergonic reactions should have earlier transition states and therefore shallower slopes, according to the Hammond postulate. However, this explanation should have resulted in curved correlations, given the wide range of driving forces in the studies, but this was not observed. More insight from the slopes can be derived from the Marcus-type analysis in the next section.

IV. Marcus-Theory and Valence Bond Analyses of Reorganization Energies. A model based on Marcus theory has been shown by one of us to reasonably well predict many HAT rate constants, within an order of magnitude or two.^{3b,58} In the $\Delta G^\ddagger_{\text{HAT}}$ vs. $\Delta G^\circ_{\text{HAT}}$ plot displayed in Figure 3, the line for the *saturated* substrates is very well described by this model. The reorganization energy λ can be estimated in two different ways. The best fit of the set of *saturated* points ($\Delta G^\ddagger_{\text{HAT}}$, $\Delta G^\circ_{\text{HAT}}$) to equation 2 (black dashed curve in Figure 3) gives $\lambda = 58 \pm 1$ kcal mol⁻¹. Alternatively, extrapolating the linear correlation to $\Delta G^\circ_{\text{HAT}} = 0$ gives $\Delta G^\ddagger_0 = 13.9 \pm 0.6$ kcal mol⁻¹ which is $\lambda/4$, giving $\lambda = 56 \pm 2$ kcal mol⁻¹. The agreement between these values and with the data points show that the simple Marcus model fits these data very well. We emphasize that this good fit is a significant result, not just a fitting exercise: the correlation line has two variables (slope and intercept) while the Marcus equation (eq 2) has a specific functional form and only a single parameter (λ). The single λ sets both the width and intercept of the Marcus parabola for $\Delta G^\ddagger_{\text{HAT}}$. The success of the simple Marcus model is remarkable.

However, this Marcus-theory model with a constant λ *does not* describe the data for the *unsaturated* substrates. The best-fit of eq 2 to the *unsaturated* data (blue dashed curve in Figure 3) is much too steep. The fit has $\lambda = 76 \pm 1$ kcal mol⁻¹, dramatically higher than the extrapolation from the linear fit to get $\Delta G^\ddagger_0(\text{unsaturated}) = 14.3 \pm 0.7$ kcal mol⁻¹, which would imply $\lambda = 57 \pm 3$ kcal mol⁻¹ (see

SI). Despite the unsaturated data being on a very different line, the $\Delta G^{\circ}_{\text{HAT}} = 0$ *intercept* for their correlation line is within error of the saturated intercept. While the Marcus fit is poor, it is clear that the unsaturated compounds must have larger λ 's since they have similar rate constants at larger driving forces. Fitting just the fastest or slowest unsaturated points to the Marcus equation gives λ values of ~ 68 or ~ 78 kcal mol⁻¹, respectively. Thus, if these data are to be fit within the Marcus picture, *the reorganization energy must vary with driving force* for the unsaturated compounds. Specifically, the λ 's for unsaturated compounds must be *greater* than the λ 's for saturated ones, and the unsaturated λ 's must increase as the C–H bonds become weaker. In this model, the increase in λ offsets the increase in driving force, leading to the shallower slope for the unsaturated substrates. This pattern of changes in λ is confirmed by computations of the Marcus inner-sphere reorganization energies λ_i using a version of Nelsen's four-point approach (see SI for details).^{59,60} The computed λ_i increased from saturated pentane (24.5 kcal mol⁻¹) to unsaturated toluene (39.1 kcal mol⁻¹) and cyclohexadiene (52.4 kcal mol⁻¹). The same trend was seen with the increase in λ_i from 2-propanol (19.7 kcal mol⁻¹) to benzyl alcohol (58.5 kcal mol⁻¹).

Unsaturated substrates having higher barriers than saturated ones was predicted by Shaik and co-workers, using semi-empirical valence bond state correlation diagrams (VBSCD).^{20,21c} This model uses vertical bond strengths $D_{\text{H-Y}}$ and reorganization energies for relaxation of the radicals ($\text{Y}\cdot$) to their preferred geometry when free ($-RE_{\text{Y}\cdot}$). The thermodynamic BDE is then $D_{\text{H-Y}} - RE_{\text{Y}\cdot}$. Using the semi-empirical VBSCD approach, they show that the “intrinsic barrier” for a HAT reaction, the barrier at zero driving force $\Delta E^{\ddagger}_{\text{VB},0}$, has a significant contribution from the RE terms (eq 4).^{21c} The VB reorganization energy and intrinsic barrier are not the same as those parameters in Marcus theory, but they are related. The RE terms for alkanes were computed to be ~ 7 kcal mol⁻¹, while those for propene, toluene and ethylbenzene were larger (16.7, 12.3 and 18.4 kcal mol⁻¹, respectively).^{21c} While not predictive in detail (ethylbenzene is more reactive than toluene), this equation captures the distinction between saturated and unsaturated substrates.

$$\Delta E^{\ddagger}_{\text{VB},0} \approx 0.05[\text{BDE}_{\text{H-X}} + \text{BDE}_{\text{H-Y}}] + 0.3[|RE_{\text{X}\cdot}| + |RE_{\text{Y}\cdot}|] \quad (4)$$

The variations in λ and the VB RE provide a qualitative connection between the PNS and Marcus models. Bernasconi himself noted that “A recurrent theme will be that high intrinsic barriers are typically associated with a lack of synchronization between concurrent reaction events such as

bond formation/cleavage, solvation/desolvation, development (loss) of resonance, etc.”.^{17c} The higher reorganization energies for HAT from benzylic/allylic C–H bonds as compared to aliphatic C–H bonds likely reflects the delocalization of the product radical in the unsaturated group, requiring bond length changes in a number of relatively high-frequency modes. Within the unsaturated group, the compounds with the weaker C–H bonds have more radical stabilization typically due to more extensive delocalization. Therefore, the reorganization energy should become larger as the $\Delta G^\circ_{\text{HAT}}$ becomes more favorable, as observed. In this picture, the PNS occurs because of the balance between energetic cost in reorganization and the favorable radical stabilization.

The Marcus and VB reorganization energies provides some intuition about the origins of some of the outliers from the correlations in Figures 2 and 3. Within the set of *saturated* substrates, for example, the largest outliers on the faster side are the most rigid ones: adamantane (**9**) and 1-aza- and 1,4-diazabicyclo[2.2.2]octanes (**46**) and (**47**). Presumably the rigidity of these substrates limits the reorganization that can occur. The point for benzaldehyde (**50**), on the other hand, falls on the saturated correlation line, a behavior that reasonably reflects the localized nature of the σ -radical formed following abstraction of the formyl hydrogen.³⁹

It is interesting to compare radical stabilization by a vinyl or aryl group with that from a heteroatom lone pair as in an amine. If it were just the presence of radical stabilization that increased λ , then the amine points would be expected to have rate constants below the saturated correlation line, but the opposite is observed: hyperconjugation places the rate constants above the correlation line. The acceleration caused by the nitrogen heteroatom does not appear to be subject to the PNS, indicating a distinction between the stabilization provided by a π -system and a heteroatom lone pair. Perhaps radical stabilization by a nitrogen lone pair does not involve substantial reorganization because the radical delocalization is quite limited, in contrast to the delocalization of the product radical in the benzylic/allylic substrates which involve a larger number of significant bond length changes.

Conclusions

An extensive experimental dataset of normalized second order rate constants k_{H}' for HAT from the C–H bonds of 56 substrates to CumO \bullet , spanning a range of more than four orders of magnitude in reactivity, has been assembled to analyze rate-bond strength correlations. Because of large discrepancies in some of the available C–H BDEs, and the absence of BDEs for some of these

substrates, a corresponding set of consistent gas-phase C–H BDEs and BDFEs spanning a range of 26 kcal mol⁻¹ has been calculated. Analysis in terms of Evans-Polanyi log k_H' vs BDE and Marcus-type $\Delta G^\ddagger_{\text{HAT}}$ vs $\Delta G^\circ_{\text{HAT}}$ plots shows in both cases the existence of two distinct correlations, one for substrates bearing benzylic and allylic C–H bonds (*unsaturated* group) and the other one for saturated hydrocarbons, alcohols, ethers, diols, amines and carbamates (*saturated* group). Such bimodal behavior supports previous results from theoretical studies of reactions promoted by other HAT reagents, and has been rationalized in terms of Bernasconi's Principle of Nonperfect Synchronization (PNS) and Marcus theory. In the unsaturated substrate group, resonance stabilization of the product radical is proportionally greater than that for the corresponding transition state and, as compared to saturated substrates, higher HAT reorganization energies are required. As a result, the significant increase in C–H BDE observed on going from benzylic and allylic to aliphatic hydrogen atom donor substrates does not translate into higher rate constants for the former group. By establishing a qualitative connection between the PNS and Marcus models, the results presented in this study expand previous findings, providing a general framework for a detailed description of the factors that govern HAT reactions from C(sp³)–H bonds, possibly representing a stimulus for a deeper understanding and for future development of this important class of reactions.

Experimental Section

Materials. Spectroscopic grade acetonitrile and isooctane were used in the kinetic experiments. 2,2-Dimethylbutane (**2**), 2,3-dimethylbutane (**3**), 2,2,3-trimethylbutane (**4**), cycloheptane (**7**), adamantane (**9**), toluene (**10**), ethylbenzene (**11**), cumene (**12**), diphenylmethane (**13**), triphenylmethane (**14**), 9,10-dihydroanthracene (**16**), diethyl ether (**22**), benzyl alcohol (**23**), 1,4-dioxane (**28**), 1-azabicyclo[2.2.2]octane (**46**), 1,4-diazabicyclo[2.2.2]octane (**47**), and benzaldehyde (**50**), were of the highest commercial quality available and were used as received. Commercial samples of propylamine (**29**), hexylamine (**31**), octylamine (**32**), triallylamine (**39**), dichloromethane (**52**) and chloroform (**53**) were purified prior of use by filtration over neutral alumina. The purity of the substrates was checked by GC prior to the kinetic experiments and was in all cases > 99.5%. Dicumyl peroxide was of the highest commercial quality available and was used as received.

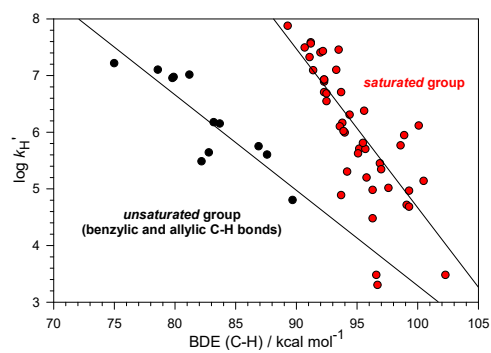
Laser flash photolysis studies. LFP experiments were carried out with a laser kinetic spectrometer using the third harmonic (355 nm) of a Q-switched Nd:YAG laser, delivering 8 ns pulses. The laser energy was adjusted to ≤ 10 mJ/pulse by the use of the appropriate filter. A 3.5 mL Suprasil quartz cell (10 mm \times 10 mm) was used in all experiments. Argon or nitrogen saturated acetonitrile or isooctane solutions of dicumyl peroxide (1.0 M) were employed. All the experiments were carried out at $T = 25 \pm 0.5$ °C under magnetic stirring. The observed rate constants (k_{obs}) were obtained by averaging 3-5 individual values and were reproducible to within 5%. Second order rate constants for the reactions of the cumyloxyl radical with the hydrogen atom donor substrates were obtained from the slopes of the k_{obs} (measured following the decay of the cumyloxyl radical visible absorption band at 490 nm) vs [substrate] plots. Correlation coefficients were generally > 0.99 . The given rate constants are the average of at least two independent experiments, with typical errors being ≤ 5 %.

Computational Methods. All calculations were performed using the Gaussian 09⁶¹ and Gaussian 16⁶² suite of programs. Conformational searches were performed using RDKit⁶³ and Hyperchem,⁶⁴ on all molecular and radical species for which there was uncertainty as to the minimum energy structure. Calculations were performed in order to determine the bond dissociation enthalpy (BDE) for the weakest C-H bond using the ROCBS-QB3 method.⁶⁵ In cases where it was feasible, W1BD⁶⁶ was used for benchmarking purposes (see the Supporting Information). In all cases, structures were verified to be local minima and possessed positive vibration frequencies. Calculation of λ_i values were performed using the B3LYP/6-311G(2d,d,p) method.^{67,68}

Acknowledgements. We thank Miquel Costas for helpful discussion and Lorenzo Stella for the use of a LFP apparatus. MS, MG and MB gratefully acknowledge financial support from the University of Rome "Tor Vergata" (Project code: E81I18000220005). E.R.-M. thanks CONACyT-Mexico for funding (scholarship Beca Extranjero 308773/472432). GAD wishes to thank the National Sciences and Engineering Research Council of Canada, the Canadian Foundation for Innovation, the British Columbia Knowledge Development Fund, and Compute Canada for generous financial support and access to computing facilities. JMM and BG gratefully acknowledge support from the US National Institutes of Health under grant R01 GM050422.

Supporting Information Available: Plots of k_{obs} vs substrate concentration for the reactions of CumO•, details of the Marcus analysis, and results of benchmarking studies on C–H BDEs. This material is available free of charge via the Internet at <http://pubs.acs.org>.

TOC Graphic



References

- ¹ Evans, M. G.; Polanyi, M. Inertia and Driving Force of Chemical Reactions. *Trans. Faraday Soc.* **1938**, *34*, 11-24.
- ² Jencks, W. P. A primer for the Bema Hypothesis. An empirical approach to the characterization of changing transition-state structures. *Chem. Rev.* **1985**, *85*, 511-527.
- ³ (a) Mayer, J. M. Hydrogen Atom Abstraction by Metal-Oxo Complexes: Understanding the Analogy with Organic Radical Reactions. *Acc. Chem. Res.* **1998**, *31*, 441-450. (b) Mayer, J. M. Understanding Hydrogen Atom Transfer: From Bond Strengths to Marcus Theory. *Acc. Chem. Res.* **2011**, *44*, 36-46.
- ⁴ (a) Kaizer, J.; Klinker, E. J.; Oh, N. Y.; Rohde, J.-U.; Song, W. J.; Stubna, A.; Kim, J.; Münck, E.; Nam, W.; Que, L., Jr. Nonheme Fe^{IV}O Complexes That Can Oxidize the C–H Bonds of Cyclohexane at Room Temperature. *J. Am. Chem. Soc.* **2004**, *126*, 472-473. (b) Wang, D.; Farquhar, E. R.; Stubna, A.; Münck, E.; Que, Jr., L. A diiron(IV) complex that cleaves strong C–H and O–H bonds. *Nature Chem.* **2009**, *1*, 145-150. (c) Xue, G.; Pokutsa, A.; Que, Jr., L. Substrate-Triggered Activation of a Synthetic [Fe₂(μ-O)₂] Diamond Core for C–H Bond Cleavage. *J. Am. Chem. Soc.* **2011**, *133*, 16657-16667. (d) Biswas, A. N.; Puri, M.; Meier, K. K.; Oloo, W. N.; Rohde, G. T.; Bominaar, E. L.; Münck, E.; Que, Jr., L. Modeling TauD-J: A High-Spin Nonheme Oxoiron(IV) Complex with High Reactivity toward C–H Bonds. *J. Am. Chem. Soc.* **2015**, *137*, 2428-2431.
- ⁵ (a) Jeong, Y. J.; Kang, Y.; Han, A.-R.; Lee, Y.-M.; Kotani, H.; Fukuzumi, S.; Nam, W. Hydrogen Atom Abstraction and Hydride Transfer Reactions by Iron(IV)–Oxo Porphyrins. *Angew. Chem. Int. Ed.* **2008**, *47*, 7321-7324. (b) Kojima, T.; Nakayama, K.; Ikemura, K.; Ogura, T.; Fukuzumi, S. Formation of a Ruthenium(IV)-Oxo Complex by Electron-Transfer Oxidation of a Coordinatively Saturated Ruthenium(II) Complex and Detection of Oxygen-Rebound Intermediates in C–H Bond Oxygenation. *J. Am. Chem. Soc.* **2011**, *133*, 11692-11700. (c) Wu, X.; Seo, M. S.; Davis, K. M.; Lee, Y.-M.; Chen, J.; Cho, K.-B.; Pushkar, Y. N.; Nam, W. A Highly Reactive Mononuclear Non-Heme Manganese(IV)-Oxo Complex That Can Activate the Strong C–H Bonds of Alkanes. *J. Am. Chem. Soc.* **2011**, *133*, 20088-20091. (d) Latifi, R.; Valentine, J. S.; Nam, W.; de Visser, S. P. Predictive studies of H-atom abstraction reactions by an iron(IV)-oxo corrole cation radical oxidant. *Chem. Commun.* **2012**, *48*, 3491-3493. (e) Vardhaman, A. K.;

Barman, P.; Kumar, S.; Sastri, C. V.; Kumar, D.; de Visser, S. P. Comparison of the Reactivity of Nonheme Iron(IV)–Oxo versus Iron(IV)–Imido Complexes: Which is the Better Oxidant? *Angew. Chem. Int. Ed.* **2013**, *52*, 12288-12292. (f) Dhuri, S. N.; Cho, K.-B.; Lee, Y.-M.; Shin, S. Y.; Kim, J. H.; Mandal, D.; Shaik, S.; Nam, W. Interplay of Experiment and Theory in Elucidating Mechanisms of Oxidation Reactions by a Nonheme Ru^{IV}O Complex. *J. Am. Chem. Soc.* **2015**, *137*, 8623-8632. (g) Mandal, D.; Shaik, S. Interplay of Tunneling, Two-State Reactivity, and Bell-Evans-Polanyi Effects in C–H Activation by Nonheme Fe(IV)O Oxidants. *J. Am. Chem. Soc.* **2016**, *138*, 2094-2097.

⁶ (a) Bryant, J. R.; Mayer, J. M. Oxidation of C-H Bonds by [(bpy)₂(py)Ru^{IV}O]²⁺ Occurs by Hydrogen Atom Abstraction. *J. Am. Chem. Soc.* **2003**, *125*, 10351-10361. (b) Matsuo, T.; Mayer, J. M. Oxidations of NADH Analogues by *cis*-[Ru^{IV}(bpy)₂(py)(O)]²⁺ Occur by Hydrogen-Atom Transfer Rather than by Hydride Transfer. *Inorg. Chem.* **2005**, *44*, 2150-2158. (c) Cho, K.; Leeladee, P.; McGown, A. J.; DeBeer, S.; Goldberg, D. P. A High-Valent Iron-Oxo Corrolazine Activates C–H Bonds via Hydrogen-Atom Transfer. *J. Am. Chem. Soc.* **2012**, *134*, 7392-7399. (d) Ghosh, M.; Singh, K. K.; Panda, C.; Weitz, A.; Hendrich, M. P.; Collins, T. J.; Dhar, B. B.; Sen Gupta, S. Formation of a Room Temperature Stable Fe^V(O) Complex: Reactivity Toward Unactivated C–H Bonds. *J. Am. Chem. Soc.* **2014**, *136*, 9524-9527. (e) Ottenbacher, R. V.; Talsi, E. P.; Bryliakov, K. P. Mechanism of Selective C–H Hydroxylation Mediated by Manganese Aminopyridine Enzyme Models. *ACS Catal.* **2015**, *5*, 39-44. Dhar, D.; Tolman, W. B. Hydrogen Atom Abstraction from Hydrocarbons by a Copper(III)-Hydroxide Complex. *J. Am. Chem. Soc.* **2015**, *137*, 1322-1329. (f) Gao, H.; Groves, J. T. Fast Hydrogen Atom Abstraction by a Hydroxo Iron(III) Porphyrine. *J. Am. Chem. Soc.* **2017**, *139*, 3938-3941. (g) Rice, D. B.; Massie, A. A.; Jackson, T. A. Manganese-Oxygen Intermediates in O–O Bond Activation and Hydrogen-Atom Transfer Reactions. *Acc. Chem. Res.* **2017**, *50*, 2706-2717. (h) Shing, K.-P.; Cao, B.; Liu, Y.; Lee, H. K.; Li, M.-D.; Phillips, D. L.; Chang, X.-Y.; Che, C.-M. Arylruthenium(III) Porphyrin-Catalyzed C–H Oxidation and Epoxidation at Room Temperature and [Ru^V(Por)(O)(Ph)] Intermediate by Spectroscopic Analysis and Density Functional Theory Calculations. *J. Am. Chem. Soc.* **2018**, *140*, 7032-7042. (i) Eshchenko, M. A.; Quist, D. A.; Karlin, K. D. Enhanced Rates of C–H Bond Cleavage by a Hydrogen-Bonded Synthetic Heme High-Valent Iron(IV) Oxo Complex. *J. Am. Chem. Soc.* **2019**, *141*, 12558-12569. (j) Fisher, K. J.; Feuer, M. L.; Lant, H. M.

-
- C.; Mercado, B. Q.; Crabtree, R. H.; Brudvig, G. W. Concerted proton-electron transfer oxidation of phenols and hydrocarbons by a high-valent nickel complex. *Chem. Sci.* **2020**, *11*, 1683-1690.
- ⁷ Koshino, N.; Cai, Y.; Espenson, J. H. Kinetic Study of the Phthalimide *N*-Oxyl (PINO) Radical in Acetic Acid. Hydrogen Abstraction from C-H Bonds and Evaluation of O-H Bond Dissociation Energy of *N*-Hydroxyphthalimide. *J. Phys. Chem. A* **2003**, *107*, 4262-4267. (b) Brandi, P.; Galli, C.; Gentili, P. Kinetic Study of the Hydrogen Abstraction Reaction of the Benzotriazole-*N*-oxyl Radical (BTNO) with H-Donor Substrates. *J. Org. Chem.* **2005**, *70*, 9521-9528.
- ⁸ Larsen, A. S.; Wang, K.; Lockwood, M. A.; Rice, G. L.; Won, T.-J.; Lovell, S.; Sadílek, M.; Tureček, F.; Mayer, J. M. Hydrocarbon Oxidation by Bis- μ -oxo Manganese Dimers: Electron Transfer, Hydride Transfer, and Hydrogen Atom Transfer Mechanisms. *J. Am. Chem. Soc.* **2002**, *124*, 10112-10123.
- ⁹ (a) Minakata, D.; Crittenden, J. Linear free energy relationships between the aqueous phase hydroxyl radical (HO \bullet) reaction rate constants and the free energy of activation. *Environ. Sci. Technol.* **2011**, *45*, 3479-3486. (b) Minakata, D.; Li, K.; Westerhoff, P.; Crittenden, J. Development of a group contribution method to predict aqueous phase hydroxyl radical (HO \bullet) reaction rate constants. *Environ. Sci. Technol.* **2009**, *43*, 6220-6227.
- ¹⁰ Hydrogen atom abstraction from C-H bonds of benzylamides by the aminoxyl radical BTNO: A kinetic study. Coniglio, A.; Galli, C.; Gentili, P.; Vadalà, R. *Org. Biomol. Chem.* **2009**, *7*, 155-160.
- ¹¹ de Visser, S. P.; Kumar, D.; Cohen, S.; Shacham, R.; Shaik, S. A Predictive Pattern of Computed Barriers for C-H Hydroxylation by Compound I of Cytochrome P450. *J. Am. Chem. Soc.* **2004**, *126*, 8362-8363.
- ¹² Tedder, J. M. Which Factors Determine the Reactivity and Regioselectivity of Free Radical Substitution and Addition Reactions? *Angew. Chem. Int. Ed.* **1982**, *21*, 401-410.
- ¹³ For additional examples of the breakdown of the EP relationship see: (a) Poutsma, M. L. Comparison of mechanistic models for correlation of activation energies of liquid-phase addition of carbon-centered radicals to terminal olefins. *J. Phys. Org. Chem.* **2008**, *21*, 758-782. (b) Molecule-Induced Alkane Homolysis with Dioxiranes. *J. Am. Chem. Soc.* **2001**, *123*, 11248-11252. (c) Bartoszek, F. E.; Manos, D. M.; Polanyi, J. C. Effect of changing reagent energy. X. Vibrational threshold energies for alternative reaction paths $\text{HF}(\nu)+\text{D}\rightarrow\text{F}+\text{HD}$ and $\rightarrow\text{H}+\text{DF}$. *J. Chem. Phys.* **1978**, *69*, 933-935.

-
- ¹⁴ Massie, A. A.; Sinha, A.; Parham, J. D.; Nordlander, E.; Jackson, T. A. Relationship between Hydrogen-Atom Transfer Driving Force and Reaction Rates for an Oxomanganese(IV) Adduct. *Inorg. Chem.* **2018**, *57*, 8253-8263.
- ¹⁵ Finn, M.; Friedline, R.; Suleman, N. K.; Wohl, C. J.; Tanko, J. M. Chemistry of the *t*-Butoxyl Radical: Evidence that Most Hydrogen Abstractions from Carbon are Entropy-Controlled. *J. Am. Chem. Soc.* **2004**, *126*, 7578-7584.
- ¹⁶ Liu, F.; Yang, Z.; Yu, Y.; Mei, Y.; Houk, K. N. Bimodal Evans–Polanyi Relationships in Dioxirane Oxidations of sp^3 C–H: Non-perfect Synchronization in Generation of Delocalized Radical Intermediates. *J. Am. Chem. Soc.* **2017**, *139*, 16650-16656.
- ¹⁷ (a) Bernasconi, C. F.; The principle of nonperfect synchronization: recent developments. *Adv. Phys. Org. Chem.* **2010**, *44*, 223-324. (b) Bernasconi, C. F.; The Principle of Nonperfect Synchronization: More Than a Qualitative Concept? *Acc. Chem. Res.* **1992**, *25*, 9-16. (c) Bernasconi, C. F.; Intrinsic Barriers of Reactions and the Principle of Nonperfect Synchronization. *Acc. Chem. Res.* **1987**, *20*, 301-308.
- ¹⁸ The PNS approach has been also used in different contexts. See for example: ref. 17a and references therein, and Harris, N.; Wei, W.; Saunders, Jr., W. H.; Shaik, S. Origins of Nonperfect Synchronization in the Lowest-Energy Path of Identity Proton Transfer Reactions Leading to Delocalized Anions: A VBSCF Study. *J. Am. Chem. Soc.* **2000**, *122*, 6754-6758.
- ¹⁹ Korzekwa, K. R.; Jones, J. P.; Gillette, J. R. Theoretical Studies on Cytochrome P-450 Mediated Hydroxylation: A Predictive Model for Hydrogen Atom Abstractions. *J. Am. Chem. Soc.* **1990**, *112*, 7042-7046.
- ²⁰ Usharani, D.; Lai, W.; Li, C.; Chen, H.; Danovich, D.; Shaik, S. A tutorial for understanding chemical reactivity through the valence bond approach. *Chem. Soc. Rev.* **2014**, *43*, 4968-4988.
- ²¹ For additional examples where such a bimodal behavior was predicted, based on the delocalization penalty see: (a) Stuyver, T.; De Proft, F.; Geerlings, P.; Shaik, S. How Do Local Reactivity Descriptors Shape the Potential Energy Surface Associated with Chemical Reactions? The Valence Bond Delocalization Perspective. *J. Am. Chem. Soc.* **2020**, *142*, 10102-10113. (b) Borden, W. T.; Hoffmann, R.; Stuyver, T.; Chen, B. Dioxygen: What Makes This Triplet Diradical Kinetically Persistent. *J. Am. Chem. Soc.* **2017**, *139*, 9010-9018. (c) Lai, W.; Li, C.; Chen, H.; Shaik, S. Hydrogen-Abstraction Reactivity Patterns from A to Y: The Valence Bond Way. *Angew. Chem. Int. Ed.* **2012**, *51*, 5556-5578.

-
- ²² (a) Markle, T. F.; Darcy, J. W.; Mayer, J. M. A new strategy to efficiently cleave and form C–H bonds using proton-coupled electron transfer. *Sci. Adv.* **2018**, *4*, eaat5776. (b) Darcy, J. W.; Kolmar, S. S.; Mayer, J. M. Transition State Asymmetry in C–H Bond Cleavage by Proton-Coupled Electron Transfer. *J. Am. Chem. Soc.* **2019**, *141*, 10777-10787.
- ²³ (a) Bím, D.; Maldonado-Domínguez, M.; Rulíšek, L.; Srnec, M. Beyond the classical thermodynamic contributions to hydrogen atom abstraction reactivity. *Proc. Natl. Acad. Sci. USA* **2018**, *115*, E10287–E1029. (b) Bím, D.; Maldonado-Domínguez, M.; Fučík, R.; Srnec, M. Dissecting the Temperature Dependence of Electron-Proton Transfer Reactivity. *J. Phys. Chem. C* **2019**, *123*, 21422-21428.
- ²⁴ (a) Goetz, M. K.; Anderson, J. S. Experimental Evidence for pKa-Driven Asynchronicity in C–H Activation by a Terminal Co(III)-Oxo Complex. *J. Am. Chem. Soc.* **2019**, *141*, 4051-4062. (b) Schneider, J. E.; Goetz, M. K.; Anderson, J. S. Statistical analysis of C–H activation by oxo complexes supports diverse thermodynamic control over reactivity. *Chem. Sci.* **2021**, *12*, 4173-4183.
- ²⁵ (a) Qiu, G.; Knowles, R. R. Rate-Driving Force Relationships in the Multisite-PCET Activation of Ketones. *J. Am. Chem. Soc.* **2019**, *141*, 2721-2730. (b) Qiu, G.; Knowles, R. R. Understanding Chemoselectivity in Proton-Coupled Electron Transfer: A Kinetic Study of Amide and Thiol Activation. *J. Am. Chem. Soc.* **2019**, *141*, 16574-16578.
- ²⁶ Costas, M.; Bietti, M. Uncovering the Complexity of the Simplest Atom Transfer Reaction. *Acc. Chem. Res.* **2018**, *51*, 2601-2602.
- ²⁷ (a) Ortiz de Montellano, P. R. Hydrocarbon Hydroxylation by Cytochrome P450 Enzymes. *Chem. Rev.* **2010**, *110*, 932-948. (b) Yin, H.; Xu, L.; Porter, N. A. Free Radical Lipid Peroxidation: Mechanisms and Analysis. *Chem. Rev.* **2011**, *111*, 5944-5972. (c) Zielinski, Z. A. M.; Pratt, D. A. Lipid Peroxidation: Kinetics, Mechanisms, and Products. *J. Org. Chem.* **2017**, *82*, 2817-2825.
- ²⁸ (a) White, M. C.; Zhao, J. Aliphatic C–H Oxidations for Late-Stage Functionalization. *J. Am. Chem. Soc.* **2018**, *140*, 13988-14009. (b) Ravelli, D.; Fagnoni, M.; Fukuyama, T.; Nishikawa, T.; Ryu, I. Site-Selective C–H Functionalization by Decatungstate Anion Photocatalysis: Synergistic Control by Polar and Steric Effects Expands the Reaction Scope. *ACS Catal.* **2018**, *8*, 701-713. (c) Li, J.; Zhang, Z.; Wu, L.; Zhang, W.; Chen, P.; Lin, Z.; Liu, G. Site-specific allylic C–H bond functionalization with a copper-bound N-centred radical. *Nature* **2019**, *574*, 516-521. (d) Wang, Y.; Carder, H. M.; Wendlandt, A. E. Synthesis of rare sugar isomers through site-selective

epimerization. *Nature* **2020**, *578*, 403-408. (e) Vasilopoulos, A.; Krska, S. W.; Stahl, S. S. C(sp³)-H methylation enabled by peroxide photosensitization and Ni-mediated radical coupling. *Science* **2021**, *372*, 398-403.

²⁹ (a) Salamone, M.; Bietti, M. Tuning Reactivity and Selectivity in Hydrogen Atom Transfer from Aliphatic C-H Bonds to Alkoxyl Radicals: Role of Structural and Medium Effects. *Acc. Chem. Res.* **2015**, *48*, 2895-2903. (b) Milan, M.; Salamone, M.; Costas, M.; Bietti, M. The Quest for Selectivity in Hydrogen Atom Transfer Based Aliphatic C-H Bond Oxygenation. *Acc. Chem. Res.* **2018**, *51*, 1984-1995.

³⁰ Salamone, M.; Bietti, M. Reaction Pathways of Alkoxyl Radicals. The Role of Solvent Effects on C-C Bond Fragmentation and Hydrogen Atom Transfer Reactions. *Synlett* **2014**, *25*, 1803-1816.

³¹ Luo, Y.-R. Comprehensive Handbook of Chemical Bond Energies; CRC Press: Boca Raton, FL, 2007, pp 19-145.

³² Salamone, M.; Basili, F.; Mele, R.; Cianfanelli, M.; Bietti, M. Reactions of the Cumyloxyl Radical with Secondary Amides. The Influence of Steric and Stereoelectronic Effects on the Hydrogen Atom Transfer Reactivity and Selectivity. *Org. Lett.* **2014**, *16*, 6444-6447.

³³ Weber, M.; Fischer, H. Absolute Rate Constants for the β -Scission and Hydrogen Abstraction Reactions of the tert-Butoxyl Radical and for Several Radical Rearrangements: Evaluating Delayed Radical Formations by Time-Resolved Electron Spin Resonance. *J. Am. Chem. Soc.* **1999**, *121*, 7381-7388.

³⁴ Avila, D. V.; Brown, C. E.; Ingold, K. U.; Lusztyk, J. Solvent Effects on the Competitive β -Scission and Hydrogen Atom Abstraction Reactions of the Cumyloxyl Radical. Resolution of a Long-Standing Problem. *J. Am. Chem. Soc.* **1993**, *115*, 466-470.

³⁵ Salamone, M.; DiLabio, G. A.; Bietti, M. Hydrogen Atom Abstraction Selectivity in the Reactions of Alkylamines with the Benzyloxyl and Cumyloxyl Radicals. The Importance of Structure and of Substrate Radical Hydrogen Bonding. *J. Am. Chem. Soc.* **2011**, *133*, 16625-16634.

³⁶ Griller, D.; Ingold, K. U. Abstraction of the hydroxylic hydrogen of alcohols by alkoxy radicals. *J. Am. Chem. Soc.* **1974**, *96*, 630-632.

³⁷ Salamone, M.; Martella, R.; Bietti, M. Hydrogen Abstraction from Cyclic Amines by the Cumyloxyl and Benzyloxyl Radicals. The Role of Stereoelectronic Effects and of Substrate/Radical Hydrogen Bonding. *J. Org. Chem.* **2012**, *77*, 8556-8561.

-
- ³⁸ Salamone, M.; Basili, F.; Bietti, M. Reactivity and Selectivity Patterns in Hydrogen Atom Transfer from Amino Acid C–H Bonds to the Cumyloxyl Radical: Polar Effects as a Rationale for the Preferential Reaction at Proline Residues. *J. Org. Chem.* **2015**, *80*, 3643-3650.
- ³⁹ Chatgililoglu, C.; Lunazzi, L.; Macciantelli, D.; Placucci, G. Absolute Rate Constants for Hydrogen Abstraction from Aldehydes and Conformational Studies of the Corresponding Aromatic Acyl Radicals. *J. Am. Chem. Soc.* **1984**, *106*, 5252-5256.
- ⁴⁰ Bardin, C.; Barton, D. H. R.; Hu, B.; Rojas-Wahl, R.; Taylor, D. K. The Fe^{II}-Fe^{IV} and Fe^{III}-Fe^V Manifolds in an Expanded World of Gif Chemistry. *Tetrahedron Lett.* **1994**, *35*, 5805-5808.
- ⁴¹ Salamone, M.; Carboni, G.; Bietti, M. Fine Control over Site and Substrate Selectivity in Hydrogen Atom Transfer-Based Functionalization of Aliphatic C–H Bonds. *J. Org. Chem.* **2016**, *81*, 9269-9278.
- ⁴² Salamone, M.; Ortega, V. B.; Bietti, M. Enhanced Reactivity in Hydrogen Atom Transfer from Tertiary Sites of Cyclohexanes and Decalins via Strain Release: Equatorial C–H Activation vs Axial C–H Deactivation. *J. Org. Chem.* **2015**, *80*, 4710-4715.
- ⁴³ Bietti, M.; Martella, R.; Salamone, M. Understanding Kinetic Solvent Effects on Hydrogen Abstraction Reactions from Carbon by the Cumyloxyl Radical. *Org. Lett.* **2011**, *13*, 6110-6113.
- ⁴⁴ Bietti, M.; Salamone, M. Kinetic Solvent Effects on Hydrogen Abstraction Reactions from Carbon by the Cumyloxyl Radical. The Role of Hydrogen Bonding. *Org. Lett.* **2010**, *12*, 3654-3657.
- ⁴⁵ Salamone, M.; Ortega, V. B.; Martin, T.; Bietti, M. Hydrogen Atom Transfer from Alkanols and Alkanediols to the Cumyloxyl Radical: Kinetic Evaluation of the Contribution of α -C–H Activation and β -C–H Deactivation. *J. Org. Chem.* **2018**, *83*, 5539-5545.
- ⁴⁶ Salamone, M.; DiLabio, G. A.; Bietti, M. Hydrogen Atom Abstraction Reactions from Tertiary Amines by Benzyloxyl and Cumyloxyl Radicals: Influence of Structure on the Rate-Determining Formation of a Hydrogen-Bonded Prereaction Complex. *J. Org. Chem.* **2011**, *76*, 6264-6270.
- ⁴⁷ Salamone, M.; DiLabio, G. A.; Bietti, M. Reactions of the Cumyloxyl and Benzyloxyl Radicals with Strong Hydrogen Bond Acceptors. Large Enhancements in Hydrogen Abstraction Reactivity Determined by Substrate/Radical Hydrogen Bonding. *J. Org. Chem.* **2012**, *77*, 10479-10487.
- ⁴⁸ Roberts, B. P. Polarity-Reversal Catalysis of Hydrogen-Atom Abstraction Reactions: Concepts and Applications in Organic Chemistry. *Chem. Soc. Rev.* **1999**, *28*, 25-35.

-
- ⁴⁹ Pischel, U.; Nau, W. M. Switch-Over in Photochemical Reaction Mechanism from Hydrogen Abstraction to Exciplex-Induced Quenching: Interaction of Triplet-Excited versus Singlet-Excited Acetone versus Cumyloxyl Radicals with Amines. *J. Am. Chem. Soc.* **2001**, *123*, 9727-9737.
- ⁵⁰ Linstrom, P. J.; Mallard, W. G. NIST Chemistry WebBook, NIST Standard Database Number 69. National Institute of Standards and Technology: Gaithersburg, Maryland, US. <https://webbook.nist.gov/chemistry/>. Date of access: December 2020.
- ⁵¹ We note, however, that the vibrational contribution to the enthalpies and free energies were determined using the harmonic approximation for all modes. Larger deviations between BDEs and BDFEs may be observed if a hindered rotor treatment is applied.
- ⁵² (a) Warren, J. J.; Tronic, T. A.; Mayer, J. M. Thermochemistry of Proton-Coupled Electron Transfer Reagents and its Implications. *Chem. Rev.* **2010**, *110*, 6961-7001. (b) Agarwal, R. G.; Wise, C. F.; Coste, S. C.; Groff, B. D.; Heuer, A. M.; Noh, H.; Parada, G. A.; Nichols, E. M.; Warren, J. J.; Mayer, J. M. Free Energies of Proton-Coupled Electron Transfer Reagents. Submitted to *Chem. Rev.*
- ⁵³ Griller, D.; Howard, J. A.; Marriott, P. R.; Scaiano, J. C. Absolute Rate Constants for the Reactions of *tert*-Butoxyl, *tert*-Butylperoxyl, and Benzophenone Triplet with Amines: The Importance of a Stereoelectronic Effect. *J. Am. Chem. Soc.* **1981**, *103*, 619-623.
- ⁵⁴ Prat, I.; Company, A.; Postils, V.; Ribas, X.; Que, Jr., L.; Luis, J. M.; Costas, M. The Mechanism of Stereospecific C–H Oxidation by Fe(Pytacn) Complexes: Bioinspired Non-Heme Iron Catalysts Containing *cis*-Labile Exchangeable Sites. *Chem. Eur. J.* **2013**, *19*, 6724-6738.
- ⁵⁵ Chen, K.; Que, Jr., L. Stereospecific Alkane Hydroxylation by Non-Heme Iron Catalysts: Mechanistic Evidence for an Fe^V=O Active Species. *J. Am. Chem. Soc.* **2001**, *123*, 6327-6337.
- ⁵⁶ Hioe, J.; Savasci, G.; Brand, H.; Zipse, H. The Stability of C α Peptide Radicals: Why Glycyl Radical Enzymes? *Chem. Eur. J.* **2011**, *17*, 3781-3789.
- ⁵⁷ Cheniers, J. H. B.; Tong, B.; Howard, J. A. Absolute rate constants for hydrocarbon autoxidation. 25. Rate constants for hydrogen atom abstraction from alkanes by the *tert*-butylperoxy radical. Howard, J. A.; Ingold, K. U. *Can. J. Chem.* **1978**, *56*, 3047-3053. Absolute rate constants for hydrocarbon autoxidation. XVIII. Oxidation of some acyclic ethers. *Can. J. Chem.* **1970**, *48*, 873-880.
- ⁵⁸ (a) Roth, J. P.; Yoder, J. C.; Won, T.-J.; Mayer, J. M. Application of the Marcus Cross Relation to Hydrogen Atom Transfer Reactions. *Science* **2001**, *294*, 2524-2526. (b) Warren, J. J.; Mayer, J.

M. Predicting Organic Hydrogen Atom Transfer Rate Constants Using the Marcus Cross Relation. *Proc. Natl. Acad. Sci. USA* **2010**, *107*, 5282-5287. (c) Mayer, J. M. Simple Marcus-Theory-Type Model for Hydrogen-Atom Transfer/Proton-Coupled Electron Transfer. *J. Phys. Chem. Lett.* **2011**, *2*, 1481-1489.

⁵⁹ Nelsen, S. F.; Blackstock, S. C.; Kim, Y. Estimation of Inner Shell Marcus Terms for Amino Nitrogen Compounds by Molecular Orbital Calculations. *J. Am. Chem. Soc.* **1987**, *109*, 677-682.

⁶⁰ Auer, B.; Fernandez, L. E.; Hammes-Schiffer, S. Theoretical Analysis of Proton Relays in Electrochemical Proton-Coupled Electron Transfer. *J. Am. Chem. Soc.* **2011**, *133*, 8282-8292.

⁶¹ Gaussian 09, Revision D.01, Frisch, M. J.; Trucks, G. W.; Schlegel, H. B.; Scuseria, G. E.; Robb, M. A.; Cheeseman, J. R.; Scalmani, G.; Barone, V.; Mennucci, B.; Petersson, G. A.; Nakatsuji, H.; Caricato, M.; Li, X.; Hratchian, H. P.; Izmaylov, A. F.; Bloino, J.; Zheng, G.; Sonnenberg, J. L.; Hada, M.; Ehara, M.; Toyota, K.; Fukuda, R.; Hasegawa, J.; Ishida, M.; Nakajima, T.; Honda, Y.; Kitao, O.; Nakai, H.; Vreven, T.; Montgomery, J. A., Jr.; Peralta, J. E.; Ogliaro, F.; Bearpark, M.; Heyd, J. J.; Brothers, E.; Kudin, K. N.; Staroverov, V. N.; Kobayashi, R.; Normand, J.; Raghavachari, K.; Rendell, A.; Burant, J. C.; Iyengar, S. S.; Tomasi, J.; Cossi, M.; Rega, N.; Millam, J. M.; Klene, M.; Knox, J. E.; Cross, J. B.; Bakken, V.; Adamo, C.; Jaramillo, J.; Gomperts, R.; Stratmann, R. E.; Yazyev, O.; Austin, A. J.; Cammi, R.; Pomelli, C.; Ochterski, J. W.; Martin, R. L.; Morokuma, K.; Zakrzewski, V. G.; Voth, G. A.; Salvador, P.; Dannenberg, J. J.; Dapprich, S.; Daniels, A. D.; Farkas, Ö.; Foresman, J. B.; Ortiz, J. V.; Cioslowski, J.; Fox, D. J. Gaussian, Inc., Wallingford CT, 2009.

⁶² Gaussian 16, Revision B.01, Frisch, M. J.; Trucks, G. W.; Schlegel, H. B.; Scuseria, G. E.; Robb, M. A.; Cheeseman, J. R.; Scalmani, G.; Barone, V.; Petersson, G. A.; Nakatsuji, H.; Li, X.; Caricato, M.; Marenich, A. V.; Bloino, J.; Janesko, B. G.; Gomperts, R.; Mennucci, B.; Hratchian, H. P.; Ortiz, J. V.; Izmaylov, A. F.; Sonnenberg, J. L.; Williams-Young, D.; Ding, F.; Lipparini, F.; Egidi, F.; Goings, J.; Peng, B.; Petrone, A.; Henderson, T.; Ranasinghe, D.; Zakrzewski, V. G.; Gao, J.; Rega, N.; Zheng, G.; Liang, W.; Hada, M.; Ehara, M.; Toyota, K.; Fukuda, R.; Hasegawa, J.; Ishida, M.; Nakajima, T.; Honda, Y.; Kitao, O.; Nakai, H.; Vreven, T.; Throssell, K.; Montgomery, J. A., Jr.; Peralta, J. E.; Ogliaro, F.; Bearpark, M. J.; Heyd, J. J.; Brothers, E. N.; Kudin, K. N.; Staroverov, V. N.; Keith, T. A.; Kobayashi, R.; Normand, J.; Raghavachari, K.; Rendell, A. P.; Burant, J. C.; Iyengar, S. S.; Tomasi, J.; Cossi, M.; Millam, J. M.; Klene, M.;

Adamo, C.; Cammi, R.; Ochterski, J. W.; Martin, R. L.; Morokuma, K.; Farkas, O.; Foresman, J. B.; Fox, D. J. Gaussian, Inc., Wallingford CT, 2016.

⁶³ RDKit: Open-source cheminformatics; <http://www.rdkit.org>. Date of access: December 2020.

⁶⁴ HyperChem(TM) Professional 8.0, Hypercube, Inc., 1115 NW 4th Street, Gainesville, Florida 32601, USA.

⁶⁵ Wood, G. P. F.; Radom, L.; Petersson, G. A.; Barnes, E. C.; Frisch, M. J.; Montgomery Jr., J. A. A restricted-open-shell complete-basis-set model chemistry. *J. Chem. Phys.* **2006**, *125*, 094106.

⁶⁶ Barnes, E. C.; Petersson, G. A.; Montgomery Jr., J. A.; Frisch, M. J.; Martin, J. M. L. Unrestricted Coupled Cluster and Brueckner Doubles Variations of W1 Theory. *J. Chem. Theor. Comput.* **2009**, *5*, 2687-2693.

⁶⁷ Becke, A. D. Density-functional thermochemistry. III. The role of exact exchange. *J. Chem. Phys.* **1993**, *98*, 5648-5652.

⁶⁸ Lee, C.; Yang, W.; Parr, R. G. Development of the Colle-Salvetti correlation-energy formula into a functional of the electron density. *Phys. Rev. B* **1988**, *37*, 785-789.